REPORT DOCUMENTATION PAGE

Form Approved
OMB No. 0704-0188

1. AGENCY USE ONLY (Leave blank)	2. REPORT DATE	3. REPORT TYPE AND DATES COVERED
	95SEP13	FINAL Report 92JUL15 - 95JUL14

4. TITLE AND SUBTITLE
Novel Sol-Gel Composite Second Harmonic Generator and Electrooptic Modulator

5. FUNDING NUMBERS
F49620-C-92-0046
63218C
1602/01

6. AUTHOR(S)
Ryszard Burzynski, Martin Casstevens, and Saswati Ghosal

7. PERFORMING ORGANIZATION NAME(S) AND ADDRESS(ES)
Laser Photonics Technology, Inc.
1576 Sweet Home Rd
Amherst, NY 14228

8. PERFORMING ORGANIZATION REPORT NUMBER
P2A-Final

9. SPONSORING/MONITORING AGENCY NAME(S) AND ADDRESS(ES)
USAF, AFMC
Air Force Office of Scientific Research /NL
110 Duncan Avenue, Suite B115
Bolling AFB, DC 20332-0001
Dr. Charles Y-C. Lee

10. SPONSORING/MONITORING AGENCY REPORT NUMBER
AFOSR-TR-95
0578

11. SUPPLEMENTARY NOTES

12a. DISTRIBUTION/AVAILABILITY STATEMENT
Approved for public release; distribution unlimited.

12b. DISTRIBUTION CODE

19951002 002

13. ABSTRACT (Maximum 200 words)

The development of organic-inorganic second-order nonlinear optical materials is discussed in light of the need to obtain practical (high performance, stable operation, processable and low cost) alternatives to inorganic crystals. Sol-gel materials have well established optical properties attributed to their superior purity and homogeneity. Processing methods of sol-gel materials permit the inclusion of numerous dopants to achieve final materials having variable and desirable properties. These materials have low optical losses and physical properties which are amenable to integrated optical devices. A number of chromophores and ormosil materials have been designed, synthesized, processed, and tested. Several composite materials are described which have high optical nonlinearities and low optical losses when they are prepared as optical waveguides. Many of these films demonstrate stable performance at room temperature and can be considered for selected applications. Specific recommendations for continued work in improving thermal stability are suggested.

14. SUBJECT TERMS	15. NUMBER OF PAGES
nonlinear optics, ormosils, sol-gel, composites, electrooptic, waveguide, hyperpolarizability, and polymer	70
	16. PRICE CODE

17. SECURITY CLASSIFICATION OF REPORT	18. SECURITY CLASSIFICATION OF THIS PAGE	19. SECURITY CLASSIFICATION OF ABSTRACT	20. LIMITATION OF ABSTRACT
Unclassified	Unclassified	Unclassified	

PROJECT SUMMARY

Title: Novel Sol-Gel Composite Second Harmonic Generator and Electrooptic Modulator
Principal Investigator: Dr. Ryszard Burzynski
Inclusive Dates: July 15, 1992 through July 14, 1995
Contract Number: F49620-92-C-0046
Senior Research Personnel: Ryszard Burzynski, Martin Casstevens, Yue Zhang, Saswati Ghosal, and Guang-Sheng He
Junior Research Personnel: Christopher Spencer, Xinyi Huang, John Weibel, Dale Tyczka, Maciej Orczyk and Genchuan Xu

Publications:

1. "A Novel Class of Sol-Gel Processed Inorganic Oxide: Organic Polymer Composites for Nonlinear Optics and Photonics." Yue Zhang, Paras N. Prasad, and Ryszard Burzynski, in Chemical Processing of Advanced Materials, Eds. Larry L. Hench, Jon K. West, Chapter 74, p. 825, John Wiley and Sons, Inc. Publisher, 1992.
2. "Sol-Gel Processed Inorganic Oxides: Orgainc Polymer Composites for Second-Order Nonlinear Optical Applications." Jaroslaw Zieba, Yue Zhang, Paras N. Prasad Martin K. Casstevens and Ryszard Burzynski, SPIE Proceedings of the Conference on *Nonlinear Optical Materials*, vol. 1758-41, p. 403-9, San Diego, California 1992.
3. "New Photonics Media Prepared by Sol-Gel Process." Ryszard Burzynski, Martin K. Casstevens, Yue Zhang, Jaroslaw Zieba, Paras N. Prasad, SPIE Proceedings of the Conference on *Organic and Biological Optoelectronics*, vol. 1853, p. 158, Los Angeles, January 1993.
4. "Photonics and Nonlinear Optics with Sol-Gel Processed Inorganic Glass: Organic Polymer Composites." Ryszard Burzynski, Paras N. Prasad in *Sol-Gel Optics Processing and Applications.* Ed. Lisa C. Klein, Chapter 19, pp. 417-450, Kulver Academic Publisher, Boston 1994.
5. "Novel Optical Composites: Second Order NLO Materials and Polymeric Photorefractive Materials for Optical Information Storage and Processing Applications.", Ryszard Burzynski, Martin K. Casstevens, Yue Zhang, and Saswati Ghosal, accepted for publication in *Opt. Eng.* 1995.

Abstract of Objectives and Accomplishments:

The development of organic-inorganic second-order nonlinear optical materials is discussed in light of the need to obtain practical (high performance, stable operation, processable and low cost) alternatives to inorganic crystals. Organic materials have high optical nonlinearities and low dielectric constants permitting efficient and high frequency electrooptic modulators to be fabricated. However, this class of materials have traditionally exhibited excessive optical waveguide losses and inferior temporal and thermal stability. Sol-gel materials have well established optical properties attributed to their superior purity and homogeneity. Processing methods of sol-gel materials permit the inclusion of numerous dopants to achieve final materials having variable and desirable properties. These materials have low optical losses and physical properties which are amenable to integrated optical devices. A number of chromophores and ormosil materials have been designed, synthesized, processed, and tested. Ormosils have been developed in an effort to eliminate the tendency of doped materials to phase separate, increase chromophore loading and reduce chromophore reorientation. Several composite materials are described which have high optical nonlinearities and low optical losses when they are prepared as optical waveguides. Many of these films demonstrate stable performance at room temperature and can be considered for selected applications. Specific recommendations for continued work in improving thermal stability are suggested including optimizing process conditions and the preparation of composites containing high T_g polyimides.

A. EXECUTIVE SUMMARY

Despite the availability of efficient inorganic second order nonlinear optical materials, there exists a need for more processable and inexpensive optical materials suitable for integrated optical device fabrication. In addition to cost and fabrication issues, there are other unique advantages to organic materials including higher frequency electrooptic modulation.

The basic approach undertaken at the start of this effort was to dope sol-gel materials with proven organic second order NLO chromophores. Sol-gel materials have well established optical properties attributed to their extremely high purity and homogeneity. LPT and other groups have shown that it is possible to prepare low optical loss films of waveguiding dimensions. This work was further motivated by these materials' greater compatibility with the substrate and the fact that numerous other components (inorganic and organic) could be doped into the film to introduce desirable properties.

The thermal stability of β and transparency range were tested for a series of chromophores. The earliest approach towards developing practical materials involved doping chromophores such as NPP into conventional sol-gel preparations. It was shown that films of high optical quality could be prepared using processing temperatures less than the thermal decomposition temperatures of the dopants. It was at this stage that several critical facts became evident.

In order for second order NLO materials to be useful in practical applications, the level of doping would have to be as high as possible. Doped materials have the tendency to phase separate either as a function of time and sooner when exposed to thermal cycling. This was indeed observed with heavily doped films.

Sol-gel processing involves the hydrolysis of alkoxides followed by controlled condensation. It was found that the procedures employed (temperatures, aging, solvents, etc.) had a tremendous effect upon the optical quality of the films and the retention of the second order NLO properties.

It was at this time that higher temperature performance was demanded of the proposed materials. This was done to conform to processing methodology used in the industry and the end users' expectations. Short term exposures (0.5 hr) to high temperatures (250-300 °C) were now required of the materials in order to survive device manufacturing. NLO stability at longer exposures (1000 hours) at moderately high temperatures (for example 100°C) were also demanded; these conditions accelerate the tendency of the dipoles to reorient and are therefore useful testing protocols.

The failure of the simply doped sol-gel materials to sufficiently retain their NLO properties under these conditions prompted further efforts to process these materials using more optimum methods. While fully condensed sol-gel materials are compact, rigid and therefore capable of retaining molecular orientation, this only occurs when the samples are exposed to temperatures above 500 °C - temperatures at which all organics decompose. The free volume of sol-gel materials processed at lower temperatures permitted dopant chromophores to reorient too freely.

In consultation with the Program Manager, it was decided to concentrate on materials development. The ability of sol-gel materials to confer better optical properties and prepare

waveguides having physical properties more like the substrate justified continued work with these systems.

It was decided that ormosil (organically modified silanes) approaches would likely retain the advantages of sol-gel processed materials while overcoming some of the limitations of the doped systems. Ormosils resemble traditional alkoxides, except that rather than being completely degenerate, one of the hydrolyzable alkoxy groups is replaced by an unreactive organic substituent that is retained (the chromophore in this case) throughout hydrolysis and condensation. This final technical report contains a description of LPT's efforts to design, synthesize, process, and test ormosil based materials. Following a comprehensive presentation of all the results, they are discussed with respect to device requirements. The report concludes with specific recommendations for continued work.

In conclusion, the staff of LPT has successfully designed and prepared second order materials having large $\chi^{(2)}$ values (5×10^{-7} esu) and prepared films of high optical quality (optical losses below 1 dB/cm). The NLO properties of many of these films have been demonstrated to be stable at room temperature. While having met the requirements outlined in the proposal for these materials, stability at higher temperatures will require additional effort. While none of the films prepared in this report have demonstrated sufficient SHG stability at 100 ^{0}C, it is not clear that these materials can not achieve this performance with additional work. Ormosils are complex materials to process. There are several steps involved in preparing and processing these materials each requiring that variables such as time, temperature, use of solvents, etc. be painstakingly optimized. Within the practical limitations of time and funding, these have been explored. However, it would be presumptuous to claim that all options have been exhausted. It is the opinion of the scientific staff at LPT that this approach deserves additional attention before its full potential can be realized.

Section B of this report provides a very brief review of the concept of 2nd order nonlinear optical phenomena emphasizing fundamental processes. Finally, experimental approaches to measurements of molecular hyperpolarizability β and materials susceptibility $\chi^{(2)}$ are discussed. Characterization of second-order NLO chromophores including the thermal stability of β values is described in Section C. Doped sol-gel polymer composite systems and their NLO and linear properties are discussed in Section D. Section E presents experimental results of $\chi^{(2)}$ studies of ormosil based materials and discusses their usefulness for photonics devices. Finally, Section F presents our conclusions from this effort and make our recommendations for future work. Appendix I and II illustrates the synthesis of NLO chromophores and ormosils, respectively. Appendix III describes film preparation techniques.

B. SECOND ORDER NONLINEAR OPTICAL PROCESSES - REQUIREMENTS AND APPLICATIONS

The realization of photonics technology rests on the development of materials which simultaneously satisfy many functional requirements. Polymeric structures offer this flexibility since: one can modify the polymer backbone as well as the pendant side chain. Furthermore, polymeric structures also offer flexibility at the bulk level being conformable to a variety of shapes (fibers, films, channel) required by specific device configurations. They can also be oriented by stretch orientation or electric field poling. However, most polymeric materials tend to be too optically lossy for most photonics applications. Furthermore, they do not have the surface quality offered by glasses. Glass and ceramic structures are also considered for NLO applications, although, while many inorganic oxides form excellent photonics media (very low optical losses), their optical and, specifically, nonlinear optical properties are not satisfactory for electrooptic devices.

In order to implement NLO materials to perform photonics functions such as optical frequency conversion, light control by electric field or even by another light beam, and build photonics devices (frequency convertors, light modulators, optical switches, limiters, memory storage etc.), one needs materials of high optical quality having large and stable optical nonlinearities.[1] The remainder of this section presents the fundamental equations describing the NLO phenomena investigated in this project.

Nonlinear optical materials can be classified in two different categories:

1. Molecular materials which consist of chemically bonded molecular units interacting in the bulk through weak Van der Waals interactions. In this class of materials, the optical nonlinearity is primarily derived from the molecular structure and one can define microscopic nonlinear coefficients β and γ which are the molecular equivalents of the bulk susceptibilities $\chi^{(2)}$ and $\chi^{(3)}$. Examples of molecular materials are organic crystals and polymers.[2,3]
2. Covalent and ionic bulk materials where the optical nonlinearity is a bulk effect. Examples of this class of materials include inorganic systems, multiple quantum well semiconductors, and inorganic photorefractive crystals.[2,3]

At the molecular level, the nonlinear optical response can be described in terms of dipoles induced by an applied electric field which can be expanded in the following power series:

$$(\mu-\mu_0)=\alpha\cdot E+\beta:EE+\gamma\vdots\ EEE. \qquad (1)$$

In the above equation μ and μ_0 are, respectively, the total and permanent dipole moments; the coefficients α, β and γ are linear, second and third order molecular polarizabilities, respectively, and describe the optical response of the material to the applied optical field.

To describe bulk optical nonlinear responses one can use an expansion of the bulk polarization P as follows:

$$P=\chi^{(1)}\cdot E+\chi^{(2)}:EE+\chi^{(3)}\vdots EEE+\ldots \qquad (2)$$

This expression is the bulk analog of equation (1). The terms $\chi^{(n)}$ are the n^{th} order bulk susceptibilities. The bulk susceptibilities $\chi^{(n)}$ can be derived from the corresponding molecular polarizabilities α, β and γ by using orientationally-averaged site sums with Lorentz local field corrections factors, relating the applied field to the local field at a molecular site. This leads to the following expressions:[4]

$$\chi^{(2)}(-\omega_3; \omega_1, \omega_2) = F(\omega_1)F(\omega_2)F(\omega_3) \sum_n <\beta^n(\theta, \phi)> \tag{3}$$

$$\chi^{(3)}(-\omega_4; \omega_1, \omega_2, \omega_3) = F(\omega_1)F(\omega_2)F(\omega_3)F(\omega_4) \sum_n <\gamma^n(\theta, \phi)> \tag{4}$$

Here, β^n and γ^n represent the molecular first and second hyperpolarizabilities at site n which are averaged over molecular orientations θ and ϕ and summed over all sites n. The terms $F(\omega_i)$ are the local field corrections for a wave of frequency ω_i, and is expressed, using the Lorentz approximation, by:

$$F(\omega_i) = (n_0^2(\omega_i) + 2)/3 \tag{5}$$

In the above expression, $n_0(\omega_i)$ is the linear index of refraction of the medium at frequency ω_i.

The relations (3) and (4) also impose symmetry constrains on the macroscopic arrangemet of the molecules. It is evident that for molecular systems with non-zero β coefficient (a third order tensor), the bulk second order nonlinear susceptibility $\chi^{(2)}$ will not exist in centrosymmetric bulk structures since

$$\sum_n <\beta^n(\theta, \phi)> = 0$$

Therefore, for a molecular system to give rise to a second-order effect, the conditions require that β is non-zero and the bulk structure is non-centrosymmetric.

The molecular structural requirements for second-order nonlinearities can also be extracted from simple two level model in which a molecule is assumed to have only two levels: a ground state, *g*, and an excited state, *i*. Under this assumption and far from resonance, β is given as [2]

$$\beta(-2\omega; \omega, \omega) = 3\frac{e^2}{2\hbar m} \cdot \frac{\omega_{ig}^2}{(\omega_{ig}^2 - \omega^2)(\omega_{ig}^2 - 4\omega^2)} F \cdot \Delta\mu \tag{6}$$

In the above equation, $\Delta\mu$ is the difference in a dipole moment between the excited state and the ground state and F is the oscillator strength of this transition. Thus, a molecule with the structure permitting a large change in charge distribution (large $\Delta\mu$) and whose excited state has a large oscillator strength will exhibit large β. These requirements are often met in structures having electron rich (electron donor) and electron attracting (electron acceptor) groups positioned on opposite sides of π-electron conjugated molecular framework. The very well known example of

such a structure is *para*-nitroaniline (PNA). This elementary discussion of nonlinear optic principles can be augmented by several books and reviews on the subject. Interested readers are encouraged to consult publications cited in references 1 to 5.

B.1 Experimental Studies of Optical Nonlinearities

Second-harmonic generation (SHG) and electro-optic (EO) phenomena and the two manifestations of second order nonlinear optical materials that have clear, widespread, and immediate applications. SHG is one means of frequency conversion, while the EO effect provides a tool of controlling light by the use of an electric field. These two effects can also be used in experimental procedures to conveniently assess the second-order nonlinearities of materials, regardless of their form (thin film or cystal, etc). Second-harmonic generation is a process in which the fundamental frequency of a intense laser pulse is doubled upon interacting with a nonlinear optical medium. As discussed above, this process requires noncentrosymmetric structures both at the molecular and the bulk levels. The noncentrosymmetry in amorphous materials (sol-gel processed and polymeric thin films) is achieved by an electric field poling process as discussed below.

For applications to second-order nonlinear optical devices, it is difficult to find bulk molecular materials which can be naturally grown into structures lacking an inversion center. In order to circumvent this problem, molecules with large β values are often dispersed in inert, amorphous matrices (host materials) such as polymers or sol-gel processed composites. Removal of the centrosymmetric molecular arrangement is performed by applying a strong DC electric field across the material whose temperature is raised to soften the matrix and allow the molecular dipoles to reorient in the direction of the applied field. This field is removed when the material is subsequently cooled to room temperature.

B.2. Poling Dynamics and Second-Harmonic Generation

The poled material possesses the ∞mm point group symmetry. With z as the direction of applied field, this symmetry reduces the nonvanishing components of the macroscopic susceptibility to $\chi^{(2)}_{zzz}$ and $\chi^{(2)}_{zxx}$ which, to the first order of the poling electric field, are related to the microscopic hyperpolarizability, β, by:[5]

$$\chi^{(2)}_{zzz} = 3\chi^{(2)}_{zxx} \tag{7}$$

and

$$\chi^{(2)}_{zzz}(-2\omega;\omega,\omega) = \frac{fN\mu\beta E_p}{5kT} \tag{8}$$

where $f=f^{2\omega}(f^{\omega})^2 f^0$ is the local field factor, μ is the molecular dipole moment, E_p is the poling electric field and kT is the thermal energy.

The second-harmonic intensity generated from the poled film is given by:

$$I_{2\omega} = \frac{512\pi^3}{A} t_\omega^4 T_{2\omega} d^2 t_0^2 p^2 I_\omega^2 \frac{1}{(n_{2\omega}^2 - n_\omega^2)^2} \sin^2\psi(\theta) \qquad (9)$$

where A is the area of the laser beam spot; d is the appropriate second-harmonic coefficient in the contracted notation; t_ω, $T_{2\omega}$ and t_0 are transmission factors[5]; I_ω is the fundamental laser intensity; p is the angular factor which projects the nonlinear susceptibility tensor onto the coordinate frame defined by the propagating electric field and n's are the refractive indices at the appropriate frequencies. The angular dependence term, $\psi(\theta)$, of the second-harmonic intensity, can be expressed as:

$$\psi(\theta) = (\pi L/2)(4/\lambda)(n_\omega \cos\theta_\omega - n_{2\omega}\cos\theta_{2\omega}) = \pi L/2l_c \qquad (10)$$

where $l_c = \lambda/4(n_\omega\cos\theta_\omega - n_{2\omega}\cos\theta_{2\omega})$ is the coherence length. At normal incidence, $l_c = \lambda/4(n_\omega - n_{2\omega})$.

The electrooptic modulation of light is a method by which one can modify an optical signal by applying external electric field to encode information. To the extent that this can be accomplished at high frequencies, the throughput and usefulness of the device increases. An electrooptic device consists of a material whose index of refraction can be altered within a very short time (less than a nanosecond for GHz bandwidths) by an electric field, E_j. This refractive index change along the principal axes of the index ellipsoid is given by:[6]

$$\Delta\left|\frac{1}{n_i^2}\right| = \sum_{j-1}^{3} r_{ij} E_j$$

$$or \qquad (11)$$

$$(\Delta n)_i = -\frac{n^3}{2}\sum_{j-1}^{3} r_{ij} E_j$$

where **E** is an external electric field at modulation frequency ω, and **r** is the electrooptic coefficient related to second order optical susceptibility. In poled polymeric materials or composites, this relation is given by:[2]

$$\chi_{zzz}^{(2)} \approx -\frac{n^4}{8\pi} r_{33} \qquad (12)$$

It is thus advantageous to utilize the largest element of the electrooptic tensor $\mathbf{r}_{ij}$ in order to

induce large index perturbations with the lowest possible voltage.

There are several considerations pertinent to the design of electrooptic devices.[7] First, the electrooptic materials must have a sufficiently large **r** coefficient to effectively respond to an electric field. For a real (lossy) material with a loss coefficient, α (absorption, scattering), and a refractive index, **n**, it translates to :

$$\chi^{(2)}/\mathbf{n}\alpha \geq 5 \times 10^{-7} \text{ esu/cm}^{-1} \text{ or } \mathbf{n}^3\mathbf{r}/\alpha \geq 5 \times 10^{2} \text{ pm/Vcm}^{-1}$$

Second, it is very important that the material be able to operate at frequencies as high as several tens of GHz; such bandwidths require materials with sufficiently low dielectric constants. The maximum bandwidth value can be estimated from the relation:

$$f = \frac{d}{R \epsilon \epsilon_0 A_{el}} \tag{13}$$

where **R** is the electric impedance at the modulation frequency, **d** is the gap (distance) between the electrodes, $\mathbf{A_{el}}$ is the electrode area, and ε_0 is the free space permittivity. For the bandwidth f > 10 GHz, R = 50 Ω, d = 6×10^{-4} cm and A_{el} = 5×10^{-4} cm^2, ε must be less than 10. In addition, a material's refractive index dispersion must be very small, ie. the index at the optical frequency should be roughly equal to $\varepsilon^{1/2}(\omega_0)$ at the modulating frequency. Although existing inorganic crystals offer large EO coefficients, their high dielectric constants limit their use in high frequency modulations. For example, $LiNbO_3$ has a dielectric constant of 32 and the maximum bandwidth is limited to fL = 9.6 GHz·cm.[8] *The above requirements are favorably matched by the properties of polymeric composite materials as listed in Table B1.*

B.3. Issues Relevant to Materials and Devices: Material requirements

The preceeding discussion speaks of NLO materials and their requirements in general. The desire to increase the operational frequency of EO modulators requires better materials and device designs. This section will discuss the particular material requirements more thoroughly.

A. Large electrooptic coefficient.

The value of a material's second order optical susceptibility, $\chi^{(2)}$, or more precisely electrooptic coefficient, **r**, determines the extent of the refractive index change, Δn, induced by externally applied electric field, E. It is this Δn which determines the achievable modulation depth. It its obvious that the desired Δn change is induced below the dielectric breakdown of the guiding medium. Thus, **materials with relatively large r** values are needed.

B. Fast response.

Among the materials that can be used in fast EO modulators (GHz frequencies), only materials exhibiting fast response times can be employed. The apparent limitations on the voltage modulation speeds can be resolved by carefully designing phase modulator geometries in order to minimize a phase velocity mismatch between RF and optical fields. In addition, RF loss narrows a device bandwidth and should be minimized.

C. Optical quality.

Any efficient optical device requires materials with superior optical quality to ensure that scattering losses due to impurities and structural and refractive index inhomogeneities are kept to a minimum. In addition, the material's absorption must be minimized at the working wavelengths in order to increase the material's damage threshold; this is a very important factor in optical waveguide considerations.

D. Thermal Stability Requirements.

We have briefly discussed the issues associated with thermal stability of poled structures in second order chromophore/polymer gest-host systems. The primary disadvantage with these materials is that the poled state is not permanent as in a crystal, but will have a tendency to decay over time to the randomly oriented state gradually diminishing the magnitude of the EO effect. The decay time may be very slow, but it is also *highly temperature dependent*. At the proximity of the matrices' glass transition, the chromophore reorientation becomes greatly accelerated. Thus, the poled NLO polymer can be viewed as an inherently and thermodynamically unstable system. It is then imperative to use host matrices that have a high glass transition temperature (T_g).

There are other parameters which are generally either not considered or reported for poled EO polymers; these are: temperature dependent linear refractive index, thermal coefficient of expansion, conductivity, stress-induced birefringence, etc. Uncontrolled variations of any of these parameters with temperature can have disasterous effect on the performance of actual devices.

Maintaining the aligned state of a polymer is of primary importance if such a material is to be of any use in practical devices. Table 1 lists the temperature requirements, military and commercial, for EO polymer integrated optic devices.

E. Other material requirements.

Among the other factors important for the EO waveguide modulators are: (i) suitable mechanical properties, (ii) compatibility with microlithographic procedures, and (iii) excellent environmental stability.

Thus, the important characteristics of a waveguide electrooptic modulator are the driving voltage (or the modulation voltage) for a specific modulation depth, the modulation bandwidth, the magnitude of the optical losses (insertion, scattering and absorption) and the manufacturing costs (or ease of fabrication). Each of these considerations stems directly from the properties of the waveguide material itself. Therefore, an electrooptic material must first be selected that has a high electrooptic coefficient and low optical losses.

B.4. Electrooptic Light Modulating Devices

The choice of design is based upon the required performance. The care and precision of these designs become all the more important as one attempts to design devices that operate at the highest frequencies. Different EO modulator designs are briefly presented below, followed by a more thorough discussion of the high frequency waveguide devices which are of great interest to the military and high-end commercial users.

A. Bulk EO modulator

Of the several electrooptic modulator geometries which are commonly used, the bulk optical modulator is the best known with established applications in the areas of optical

Table B1 Temperature requirements for electrooptic polymer integrated optic devices*

SPECIFICATION	Temperature (^{0}C)
Military spec 883c level 2	
Use	-40 to 125
Storage	200
Commercial	
Use	20 to 80
Storage	120
Other	
Fiber attachment	≤250
Wire bonding	≤100
Hermetic package	≤320
Subassembly	≤320

* after Ref. 8.

communication and high speed signal processing, e.g., phase array antennas. Large bandwidth operation, (1 Ghz), in a bulk configuration can be achieved. An undesirable feature of these devices is the relatively high drive powers which are required. Diffraction effects prohibit making bulk modulators with both small lateral dimensions and long interaction lengths necessary to accomplish low drive voltage operation. None-the-less, the bulk modulator parameters can still be optimized and/or be enhanced if electrooptic materials having lower dielectric constants at the RF modulation frequencies and small refractive index dispersion can be found. Furthermore, employing materials with larger electrooptic coefficients would substanitially decrease the required drive voltage.

B. Waveguide EO modulators

Waveguide electrooptic modulators are increasingly gaining importance because of their compatibility with optical fiber communication systems and because they bring the technology closer to the ultimate goal of complete device integration. The structure of a simplest channel

waveguide electrooptic modulator is shown in Figure B1. In general, a voltage **V** is applied to the electrodes placed alongside (or below and above) the waveguide. It creates an internal field **E** ≈ **V/d** where **d** is the electrode gap. The linear change in the index, $\Delta \mathbf{n}$, is induced by the externally applied electric field **E**.

There are three important parameters of a waveguide electrooptic modulator which determine its usefulness:

1) drive voltage used to achieve the desired modulation depth
2) modulation bandwidth
3) optical insertion loss

For the waveguide modulator in Figure B1, the effective index change induced by the electrooptic process is described by:[9]

$$\Delta n(V) = -(n^3 r/2)\cdot(V/d)\cdot\Phi \tag{14}$$

where Φ is the overlap integral between the applied electric field E, and the optical field

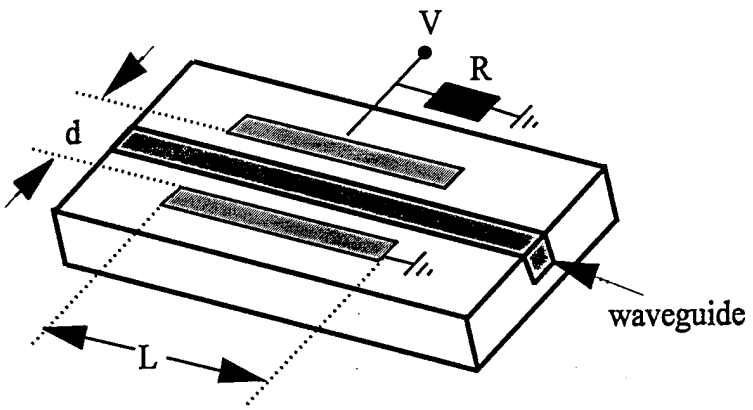

Figure B1 Waveguide electrooptic modulator

distribution, E_{op}, within the waveguide:

$$\Phi = \int\int E\,|E_{op}|^2\,dA \tag{15}$$

The common procedure in such devices is to electrically induce a phase shift $\Delta\phi$ in the optical fields on the order of π as they pass the electrooptic guiding region of length L. At an optical wavelength, λ, the potential modulator bandwidth given as $\Delta f=(\pi RC)^{-1}$ (where R is the driving source impedance and C modulator capacitance), the modulator figure of merit (driving voltage /bandwidth ratio) is expressed as follows:

$$(V/\Delta f) \approx \pi R\cdot(\epsilon_{eff}/n^3 r)\cdot\lambda\cdot(dG\kappa)/\Phi \qquad (16)$$

where $\epsilon_{eff} = (\epsilon_0/2)(1+\epsilon_s/\epsilon_0)$, G is a function of electrode parameters (width and gap) and ϵ_s is the RF dielectric constant of the material

It can be seen that both the driving voltage and the modulation bandwidth scale vary inversely with the device length. Thus, to increase the bandwidth, one may decrease the length, L, at the expense of drive voltage and vice versa. For an optimum design, a material must have a *large electrooptic coefficient, sufficiently high refractive index, low dielectric constant, and be easily processed into waveguides.*

Apart from the device geometry and modulator type, where optimization is essentially an engineering issue, proper identification or design of the device's active material is an extremely critical and difficult task. Our approach in designing and optimizing this material has relied on the sol-gel processed composites. This approach offers enormous flexibility in matching specific material parameters (index of refraction, processability, etc.) as well as control over both the linear and nonlinear optical properties. This is in contrast to commonly known crystalline materials where entirely different growth techniques must be used in fabricating different device geometries. The versatility of this method has permitted the staff of LPT, Inc. to prepare and evaluate a number of composites many of which can be used in specific device configurations.

B.5. Measurements of SHG ($\chi^{(2)}$) and Electrooptic Modulation

The second-order susceptibilities of the prepared bulk material, usually in the form of thin films cast on ITO coated glass substrates, are conveniently measured by the second-harmonic generation technique using the angular dependence method. The sample, mounted on a rotational stage, is rotated perpendicularly to the laser beam. The SHG signal is recorded as a function of the rotation angle. In order to account for transient changes in the incident laser pulses, the amplitude of the SHG signal is compared to that from a Y-cut quartz plate ($\chi^{(2)}$=1.2 x 10^{-9} esu) to calculate the second-order susceptibility of the material.

The experimental setup for SHG measurement of $\chi^{(2)}$ is presented in Figure B2. The experiment is carried out with a Q-switched Nd:YAG laser operating at 10 Hz. The SHG signal is detected by a PMT and processed by a boxcar signal processor interfaced to a personal computer.

For the electrooptic modulation experiment, the film is cast or spincoated on ITO covered glass substrates. Thin metal (Ag or Au) films are deposited on the top of the NLO material and serve as an electrode. The measurement of the electrooptic coefficient of a material is performed using the experimental setup as shown in Figure B3. When the laser beam is polarized 45° with respect to the plane of incidence, the components parallel and perpendicular to the plane of

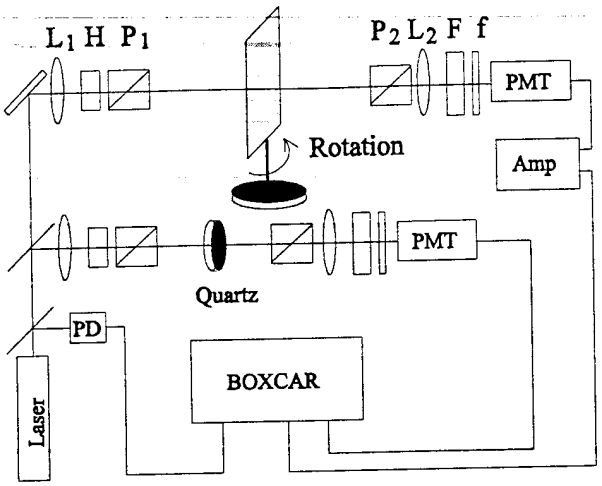

Figure B2 SHG setup

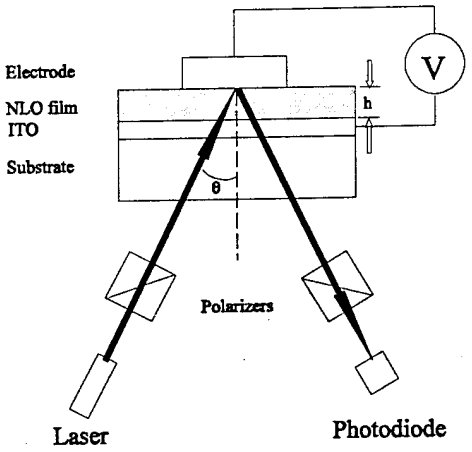

Figure B3 EO setup

incidence will experience different phase retardation. This phase retardation is related to the birefringence by[18]:

$$\phi_m = \frac{2\pi}{\lambda} d\Delta n_0 \frac{\sin^2\theta}{\cos\theta} \qquad (17)$$

Precise measurement of this phase retardation permits one to calculate the electrooptic coefficient, r, using:

$$\Delta n_0 = \frac{1}{2}(n_3^3 r_{33} - n_2^3 r_{31})\frac{V}{h} \quad (18)$$

where h is the film thickness.

B.6. The Basic Principles of The Electric-Field-Induced Second-Harmonic Generation (EFISH) Measurement of Molecular Nonlinearity

Characterization of the molecular nonlinear optical coefficients is often done in the solution phase. The random orientation of the molecules in the solution phase, cause the second-order polarizations induced by light on each individual molecule cancel each other; the second-order response is not observed. The electric-field-induced second-harmonic (EFISH) generation technique is often applied to remove the inversion symmetry in the solution phase. In this technique, the sample solution is placed in a wedge shaped cell and a strong pulsed dc electric field is applied across it, synchronously to the laser pulses, to align the molecules in the direction of the electric field. As the cell is translated across the laser beam, the second-harmonic intensity changes as a result of the change in the optical path length. An effective polarizability is obtained from the concentration dependence of both the SHG intensity and the coherence length of the solution. In order to extract the nonlinearity of the solute molecules, a series of solutions with various concentrations are prepared and the SHG fringes recorded. After numerically fitting the fringes, the amplitude and coherence length for each concentration are used to calculate the effective Γ^{EFISH} values. Thereafter, γ^{eff} values are calculated by fitting the concentration dependence according to Eq. (19).

$$\Gamma_L = f(N_A\gamma_A^{eff} + N_R\gamma_R^{eff}) \quad (19)$$

where N_A and N_R refer to the numbers of molecules of solute and solvent, respectively, per unit volume and $f = f_v^0(f_v^\omega)^2 f_v^{2\omega}$ is the local field factor. The molecular first hyperpolarizability, β, is calculated from[3]

$$\gamma_A^{eff} = \gamma^{el} + \frac{\mu\beta}{5kT} \quad (20),$$

where μ is the dipole moment, kT is the Boltzman thermal energy and γ^{el} is the electronic part of the second hyperpolarizability which can be measured by the degenerate four-wave mixing experiment. Complete details on EFISH methodology are presented in the next section.

REFERENCES

1. Prasad, P.N., (1987). *Thin Solid Films*, **152**, 275.
2. Prasad, P.N., and Williams, D.J., (1991). *Introduction to Nonlinear Optical Effects in*

Molecules and Polymers, Wiley, New York.

3. Chemla, D.S. and Zyss, J., (1987). *Nonlinear Optical Properties of Organic Molecules and Crystals*, Academic Press, New York.
4. Williams, D.J., (1988). *Angew. Chem. Int. Ed.*, **23**, 1940.
5. Singer, K.D., Kuzyk, M.G., and Sohn, J.E. (1988). In *Nonlinear Optical and Electroactive Polymers*, Eds. Prasad, P.N., and Ulrich, D.R., Plenum Press, New York.
6. Yariv, A. and Yeh, P.C. (1984). *Optical Waves in Crystals*, Wiley, New York.
7. Tamer, T., Ed., (1979). Integrated Optics, Springer-Verlag, New York.
8. Lytel, R., Libscomb, G.F., Kenney, J.T.and Binkley, E.S., (1992). In "Polymers for Lightwave and Integrated Optics: Technology and Applications" Ed. L.A. Hornok, Marcel Dekker, New York.
9. Alferness, R.C., (1982). *IEEE Trans. Microwave Theory. Tech.*, **MTT-30**, 1121.

C. SECOND-ORDER NLO CHROMOPHORES - HYPERPOLARIZABILITY AND THERMAL STABILITY

EFISH measurements are a convenient method of characterizing the second order molecular polarizability of NLO chromophores. NLO molecules in solution phase are randomly oriented and the second-harmonic signal generated from each molecule effectively cancels out.

A strong dc electric field is applied across the solution in order to bias the average orientation of the molecules. The percentage of molecules which can be aligned in the direction of electric field depends on the strength of the field. The viscosity of the solution contributes to the time required to fully align the dipoles. Since the EFISH trials typically employ pulsed E fields, special attention has been taken to eliminate the viscosity as a source of potential error.

The experimental setup is depicted in Figure C1. EFISH measurements were performed

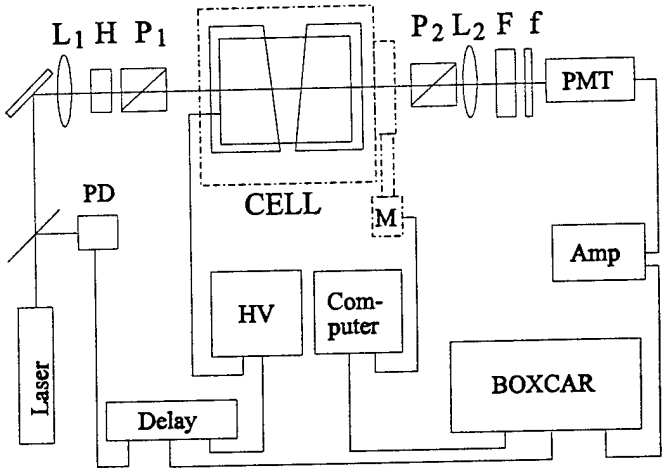

Figure C1 Experimental setup for electric field-induced second-harmonic generation.

at a wavelength of 1.064 μm using a Q-switched Nd^{+3}:YAG laser operating at 10 Hz. Each pulse at 1.064 μm has a pulse width of about 15 ns. The quarter-wave-plate and the first polarizer rotate the horizontally polarized laser beam to a vertical polarization. The second-harmonic signal generated from the sample solution was focused onto a photomultiplier tube (PMT). The signal was preamplified and then processed by an EG&G 4402 BOXCAR signal analyzer. Figure C2 shows the EFISH cell employed in the experiments. Two fused silica windows form a wedge, with an angle of 10 degrees, which contains the sample solution. These windows are sandwiched between two polished copper electrodes. The windows and the electrodes are surrounded by Teflon® to minimize the potential ohmic contacts. The cell is mounted on a motor-driven, computer controlled translational stage with a translation range of 40 mm to facilitate the path length adjustment of a laser beam traversing the solution.

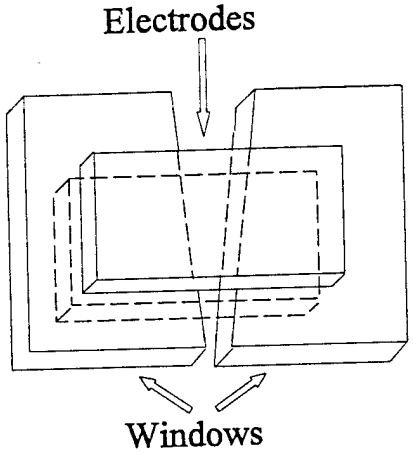

Figure C2 The EFISH cell

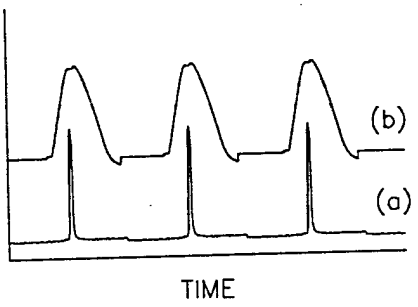

Figure C3 High voltage pulses (b) synchronized with the laser pulses (a)

A pulsed power supply (Velonex Model 350) generates high voltage pulses in the range of 0 to 30 kV with a pulse width adjustable from 1 μs to 100 μs. A pulsed voltage is used in order to minimize the probability of electrolysis or polarization of the cell windows. The high voltage pulses must be synchronized with the laser pulses to ensure that a stable voltage is applied when the laser beam interacts with the molecules. This is done by triggering each high voltage pulse about 1.99 ms after the detection of the previous laser pulse. The high voltage pulses applied to the electrodes are monitored by an oscilloscope. Figure C3 shows the HV pulses synchronized with the laser pulses. Typical HV pulses have a width of 25 μs.

The solvent(s) used in the EFISH experiment must be carefully selected according to a number of criteria. The solvent must be chemically inactive, enable sufficient concentrations of the NLO chromophore, have a well characterized Γ^{EFISH} value and be of sufficiently low viscosity to enable molecular reorientation. Different solvents have been used in the EFISH measurement of different compounds, e.g., chloroform for NPP ($\Gamma^{EFISH} = 0.88 \times 10^{-13}$ esu) and 1,4-dioxane ($\Gamma^{EFISH} = 0.5 \times 10^{-13}$ esu) for DEANST and PRODAN.

The β values for each chromophore were measured as a function of the temperature at which the sample was heated for 30 minutes. In addition, the EFISH signals were measured as a function of chromophore concentration. The maximum concentrations used for NPP, DEANST and PRODAN are 7, 0.7 and 7 mg/ml, respectively.

The measurements were carried out as follows. A series of samples of each chromophore were made by heating the samples at a number of different temperatures for 30 minutes. After

cooling them down to room temperature, EFISH measurements were carried out on each sample as described above. The temperature dependence of the EFISH β values for NPP, DEANST and PRODAN are presented in Figures C4, C5 and C6, respectively. It is clear from the data that NPP, DEANST and PRODAN experience a 10% drop in their β values at 120, 150 and 250 °C, respectively.

The combined results of these experiments are presented in Figure C7 which displays the thermal stability of the chromophores versus their figure of merit defined as:
$FOM^{SHG} = \beta / MW$, where MW denotes the molecular weight of a given chromophore.

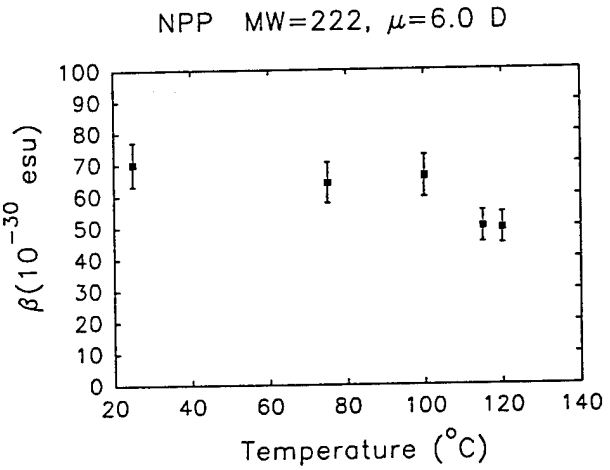

Figure C4 Dependence of β on heating temperature

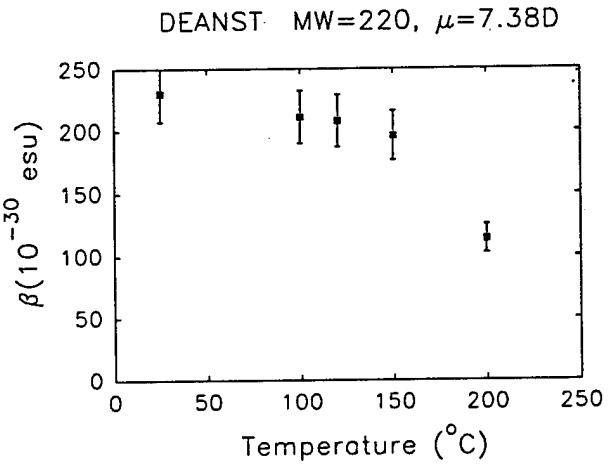

Figure C5 Dependence of β on heating temperature for DEANST

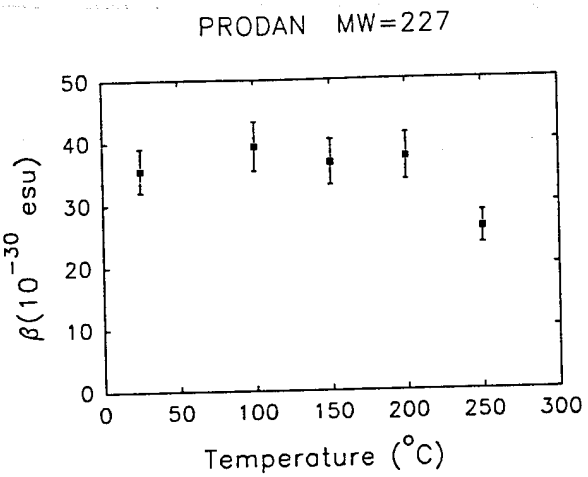

Figure C6 Dependence of β on heating temperature for PRODAN

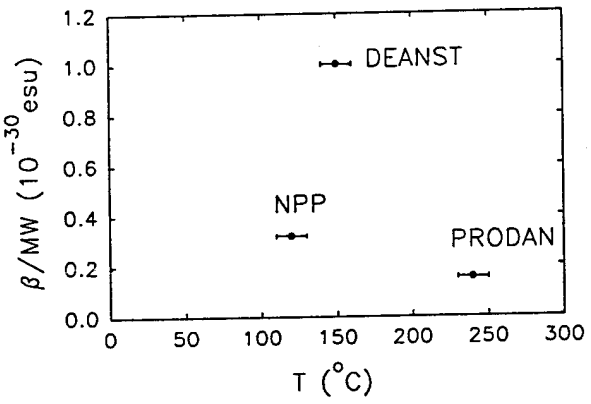

Figure C7 Plot of $FOM^{SHG} = \beta/MW$ for the studied chromophores versus temperature at which their β value is observed to decrease by 10% in air atmosphere.

It must be recognized that the above data was obtained in extreme conditions. The heated samples' exposure to oxygen will contribute to sample degradation. It is quite understandable that organic molecules possessing active groups such as amino or hydroxyl functionals may undergo chemical reaction (oxidation, partial decomposition, etc.). The same chromophore molecule, if dispersed in an inert matrix or subjected to a similar thermal treatment under dry and oxygen free atmosphere may not exibit any decrease of its molecular hyperpolarizability value at even higher temperatures.

D. DOPED SOL-GEL PROCESSED COMPOSITES

The use of sol-gel processed materials as host matricies for second order NLO chromophores has been discussed on preceeding pages. Detailed descriptions of the chemical reactions involved and properties of the resultant materials can be found in numerous publications (ref) and reports submitted on previous occasions. This section summarizes our efforts preparing and testing sol-gel materials doped with selected NLO materials. In addition to the NLO properties, selected measurements of waveguide optical losses are reported. The preparation of the NPP/SiO_2/TiO_2 (15:45:40 wt% respectively), and PNA/ PMMA/TiO_2/SiO_2 (15:20:30:35 wt% respectively) composites have been performed as described in our Phase I research reports.[a]

The preparation of the oxide/polymer/ DEANST composite was conducted as follows: hydrolysis of tetraethylorthosilicate (TEOS) was performed using a mild acid catalyst and a 2:1 molar ratio of water to TEOS. The same amount of methanol (MeOH) was introduced into the mixture as a homogenizing agent (mutual solvent). The hydrolysis and condensation reactions were allowed to proceed for 1 day at room temperature. Concurrently, a 10% solution of poly-vinylpyrrolidone (PVP) polymer in dimethylformamide (DMF) was prepared and combined with the desired amount of hydrolyzed TEOS. Finally, an appropriate amount of DEANST was added to the solution. After stirring for 15 min at room temperature, the mixture was used in the preparation of films on glass substrates (plain or ITO coated) using either a spin coating method (thin films) or doctor blading method (films of thickness greater than 1 μm). LPT employs a commercial spincoater (Headway) and a custom built "doctor blading" apparatus using a modified microtone. The glass substrates used for film deposition were carefully cleaned in an ultrasonic bath first using a base cleaning solution (KOH in isopropyl alcohol), then deionized water, acid bath, HCl in isopropyl alcohol (this step was skipped for substrates covered with ITO layers), deionized water and, finally, in spectroscopic grade isopropyl alcohol. Among several diffrent DEANST concentrations (between 10 wt% to 45 wt%) used in film preparations, we found that a 20 wt% concentration of the chromophore in sol-gel/polymer matrix was close to the maximum amount which could be dispersed to form homogeneous and stable composite material. Higher concentrations than 25 wt% usually resulted in crystallization of the DEANST after some time which depended on the amount of the incorporated DEANST; in some cases it occured two to three days after the film preparation and in other instances even after a month.

D.1. In situ Poling Second-Harmonic Generation Studies

The electric field poling efficiency depends on a large number of parameters such as the poling temperature, poling electric field, environmental humidity and the material curing processes. The optimal poling conditions vary from one material to another. In order to perform more efficient electric field poling, one has to determine the best poling conditions for each material. We have conducted numerous *in situ* poling second-harmonic generation studies on the

---

[a] Note: the relative amount of PNA in the above composite corresponds to the amount used in the film preparation. The final concentration of PNA may differ substantially from the above value because of the tendency of PNA to sublime upon drying and when poling the composite film at elevated temperatures.

sol-gel processed material composites by monitoring the SHG intensity from the material while different poling parameters are varied either individually or simultaneously.

The *in situ* SHG experiments were conducted on several of the material composites described in this report: NPP/SiO_2/TiO_2 and DEANST/PVP/SiO_2. The in-situ technique provides real-time information about the matrix and its ability to retain the chromphores in their preferred orientation. This property can change dramatically as the materials are thermally processed. In both composites, the second-order chromophores were shown to be electrically aligned at room temperature. In the NPP/SiO_2/TiO_2 composites, the decay of the second-harmonic signal was monitored as a function of heat treatment as shown in Figure D1. Curve 1(a) shows the SHG decay after heating the film to 115 °C and immediately cooling it down to room temperature at which time the field was removed. In curve (b), the film was heated at 115 °C for one hour before the field was turned off while in curve (c) the electric field was turned off after three hours of heating at 115 °C. *It is clear that, as the sample is annealed at moderate temperatures, the sol-gel films exhibits a more stable alignment of the chromophores as evidenced by a slower relaxation of the poled structure.*

The *in situ* poling studies of the DEANST/PVP/SiO_2/TiO_2 composite showed a different behavior than the chromophore/SiO_2/TiO_2 composites. The presence of the polymer (PVP) permits the SHG signal to rise faster when the sample is heated close to the glass transition temperature of PVP. Cooling the sample to room temperature relatively fast causes the SHG signal to drop even in the presence of the electric field. However, when the temperature is raised again, the SHG signal can be regained. When this sample was cooled very slowly to room temperature, most of the SHG signal (usually more than 90%) was maintained. The sample was treated with a series of temperature cycles, (as shown in Figure D2) to illustrate this phenomenon. It can be seen that the SH intensity increased slightly with each successive thermal cyde.

D.2. Second-Order Susceptibility and Stability

Table D1 lists experimental results of second-order susceptabilities obtained for the above composite materials and normalized that of Y-cut quartz crystal. Other composite properties are also listed.

The temporal stability of the poled structures at ambient conditions have been monitored for an extended period of time (100 days for the NPP composite and 30 days for the DEANST composite) by repeatedly measuring the SHG intensity. As can be seen from Figure D3, these composites show, at room temperature, stability of the field induced alignment after the poling field has been removed.

Table D1 $\chi^{(2)}$ values and chromophore number densities of the poled sol-gel composites.

Doped Chromophore	N (10^{20} cm^{-3})	$\chi^{(2)}$ (10^{-8} esu)	λ_{MAX} (nm)	Chromoph. dec. temp. (^{0}C)
PNA	~6	1.4	347	(subl.)
NPP	~6	2.6	393	310
DEANST	~9	14	432	240

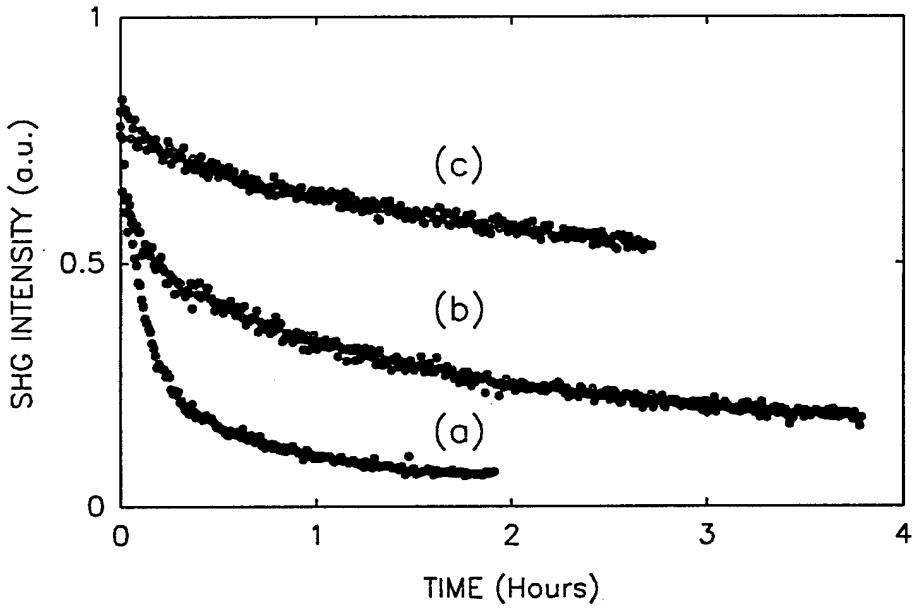

Figure D1 Effect of heat treatment on the stability of the poled structure in an NPP/SiO_2/TiO_2 composite.

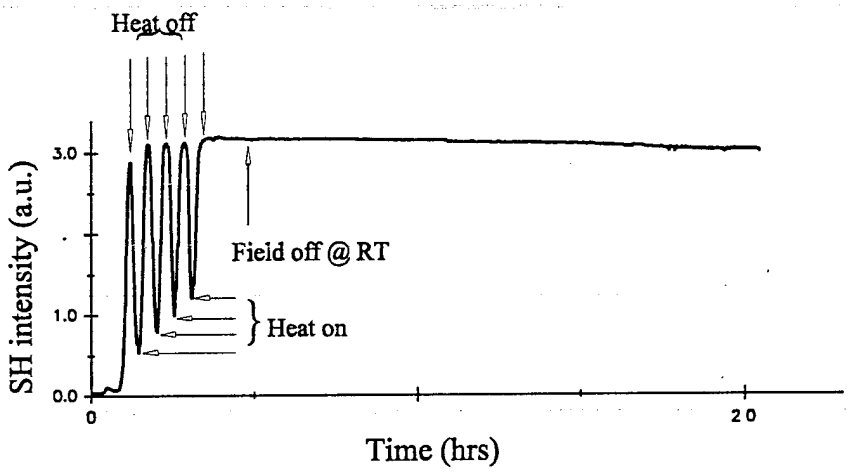

Figure D2 *In situ* poling SHG from a DEANST/PVP/SiO_2 composite

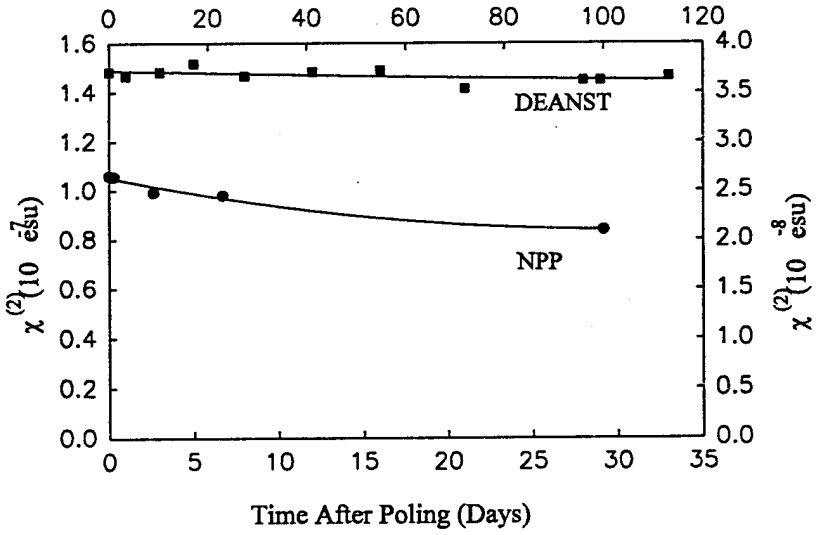

Figure D3 Temporal stability of the poled structures. DEANST/PVP/SiO_2 - lower and left axes; NPP/SiO_2/TiO_2 - upper and right axes.

D.3. Thermal Stability of the Poled Structures

The thermal stability of the induced noncentrosymmetric chromophore alignment within the sol-gel/polymer composite matrix has been tested by monitoring the intensity of the generated second-harmonic signal from the poled film at different temperatures. The field was turned off after the poling was complete and the films had cooled to room temperature. Subsequently, the film temperature was increased by 10 ^{0}C in about 3 minute intervals (up to 115 ^{0}C and 135 ^{0}C for the composites containing DEANST and NPP, respectively) and held for 30 minutes at each setting. The strength of the SH signal obtained in these measurements was normalized to those recorded for the samples poled in optimal conditions.

Figures D4 and D5 display experimental results obtained for sol-gel/polymer composites containing DEANST. The films were heated above the melting point of DEANST (95^{0}C) in both experiments and display very similar thermal behavior of the SHG signal. The small differences in temperature dependence of SH intensity for the studied films can be attributed to different doping levels and small changes in the host matrix composition. None-the-less, it is evident that the most dramatic decrease of SH intensity is observed in the vicinity of the melting point temperature of DEANST. The data presented in Figure D5 shows this behavior more clearly. The sample exhibited less than a 20% decrease in the SH signal strength after its temperature reached 90 ^{0}C. The signal remained at this level for a considerable period of time when the sample was cooled to 65 ^{0}C. The sample was then heated well above 90 ^{0}C and maintained; the onset of the dramatic decrease in SH signal can be seen at a temperature just below 100 ^{0}C and is coincident with the melting point of DEANST (96 ^{0}C). The SH signal never dropped below 20% of its original value which may indicate that a small portion of the chromophore molecules are indeed "fixed" in the orientation induced by the poling electric field. The irreversible signal loss (or loss of the chromophore alignment) at high temperatures mirrors the room temperature behavior of chromophores dispersed in polymeric matrices. These results indicate that one or more factors may be responsible for the observed behavior:

1. the thermal expansion and/or increased matrix mobility of the composite may be large; this may be due to a large content of the polymers (about 60 wt%) in the composite material
2. the chromophore molecules are not rigidly attached to silica/titania network
3. the chromophore molecules form a nanometer-sized microdomains within the host matrix.
4. The presence of an unacceptably large pore structure.

The fact that the $\chi^{(2)}$ value of composite films containing DEANST falls dramaticaly at the melting point of DEANST seems to be in agreement with number 3 above. However, DEANST crystalizes in the rhombic form having P_T symmetry; this crystal possesses an inversion center which is inconsistent with this conjecture. It should be mentioned that the solubility of DEANST in a sol-gel/polymer matrix is extremely high (doping up to 35 wt% was achieved without phase segregation) which indicates its high affinity to the host matrix. These interactions coupled with the added rigidity of the sol-gel environment are sufficient to maintain electric field poled structures for several months at room temperature; they will not, however, be strong enough to counteract molecular thermal motions at temperatures above 90 ^{0}C.

Figure D7 depicts the thermal stability of the second harmonic signal obtained from a

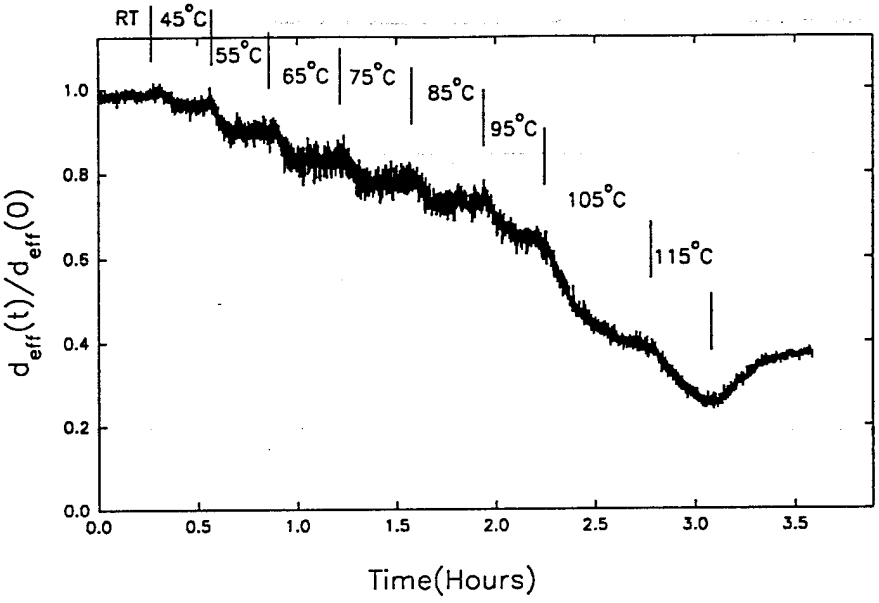

Figure D4 Stability of SH signal from DEANST/SiO_2-TiO_2/PVK,PVP electric field poled composite at different temperatures.

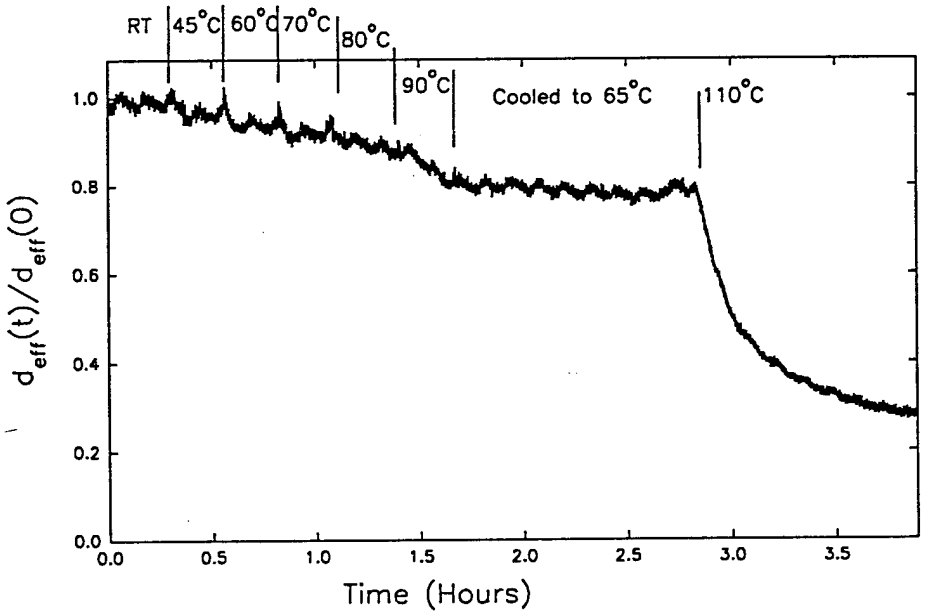

Figure D5 Stability of SH signal from the composite as in Figure D4 at different temperatures; the film was cooled to 65 0Cafter being heated close to its melting point and, the, reheated above it.

thin film of NPP/SiO_2, TiO_2/PVK, PVP composite material. The fact that the signal intensity decreased by only 5% at temperatures up to 100 °C provides additional evidence that the NPP chromophores are strongly bound to the sol-gel oxide network, most probably through its – OH group. LPT has previously demonstated evidence of such interactions in thermal studies of a NPP/SiO_2 composite by the use of DSC techniques. These studies revealed that the NPP molecules dispersed in sol-gel prepared silica decompose at a temperature of about 50°C higher (360°C) than that of pure NPP (310°C). It can also be seen in Figure D6 that, even after increasing the film temperature much above the melting point of NPP (115°C), the observed decrease of SH intensity was far more gradual than one would expect.

The presented experimental data strongly supports our contention that chromophore/sol-gel/polymer composites exhibiting very stable second-order optical structures, both thermally and temporally, can be prepared. The prerequisite to accomplish this is defined by strong interactions between chromophore molecules and the sol-gel matrix and the inherent rigidity of the oxide network.

It was argued in Section C that the measured thermal stability of the chromophores, i.e., decrease of their β values while exposed to high temperatures, can be substantially slowed down when chromophores are dispersed in polymeric matrices or films containing chromophores overcoated with another layer.

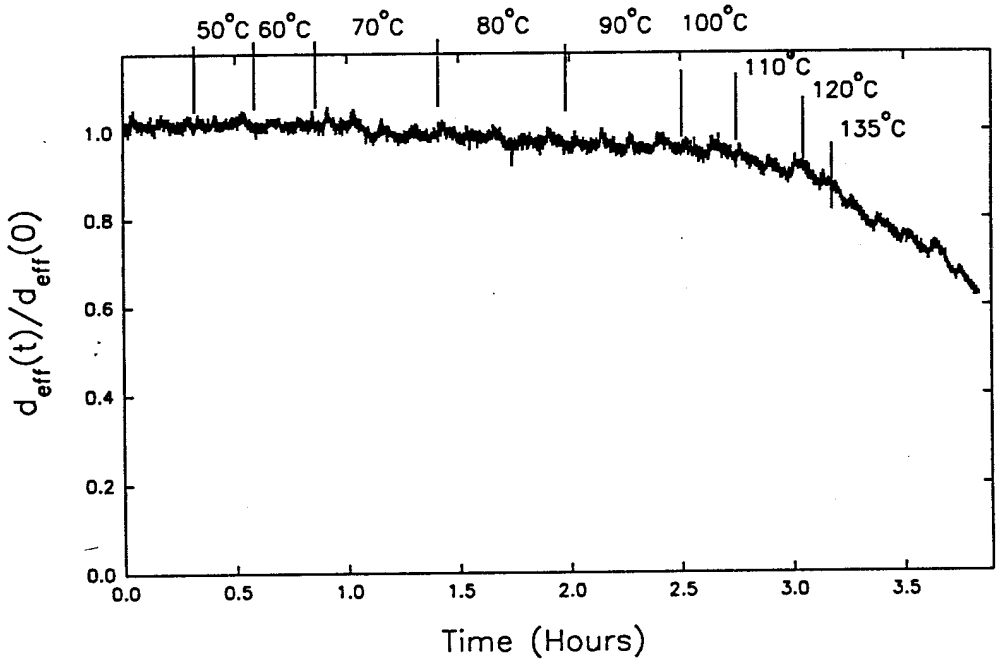

Figure D6 Thermal stability of SH signal from a poled film of sol-gel/polymer composite containing NPP chromophore.

In order to validate this proposition, we have prepared three identical sol-gel composite films doped with NPP chromophore. The first sample contained NPP heated for 1 hr in air at 150^{0}C, i.e 30 ^{0}C above the temperature at which the 10% decrease of NPP's β value was observed. NPP dispersed in the second sample had been treated simultaneously but in a dry and inert atmosphere (N_2). The third sample was doped with NPP which had not been thermally treated. All films were subsequently poled at 130 ^{0}C using corona discharge and the SHG signal strength was observed. The sol-gel films doped with untreated NPP and with NPP heated under N_2 atmosphere were found to have the same $\chi^{(2)}$ value, i.e. 2.3×10^{-8} esu, while sample doped with NPP kept in air at 150 ^{0} C exhibited $\chi^{(2)}$ value of 1.9×10^{-8} which is about 20% less than that of the other two samples. Figure D7 depicts the experimental data used in the determination of $\chi^{(2)}$ values for the above three samples.

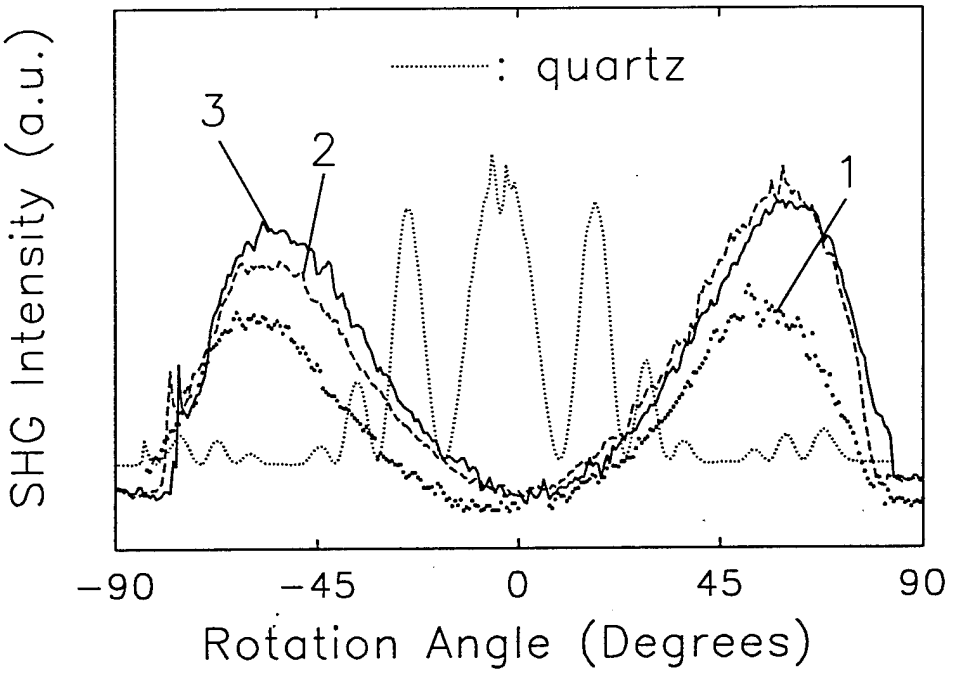

Figure D7 Angular dependence of SHG efficiency from NPP/SiO_2,TiO_2 composite films containing (1) thermally annealed NPP in air (short dashed line); (2) thermally annealed NPP in N_2 (solid line); and (3) NPP which was not thermally treated (long dashed line

In conclusion, the presented results indicate that chromophores of a relatively low thermal stability may retain their nonlinear optical properties after treatment at substantially higher temperatures providing that the thermal treatment is performed either in an inert atmosphere or the chromophore molecules are dispersed in an inactive matrix which can prevent or inhibit undesirable chemical reactions between the chromophore and oxygen. In an operational environment, overcoatings to minimize the samples' exposure to oxygen may be required in

order for some materials to meet the thermal stability requested by the Air Force.

D.4 Waveguide Losses in Sol-Gel/NLO Chromophore Composite Films

One of the primary goals of this Phase II development effort was to fabricate low optical loss second order NLO waveguides using sol-gel processed inorganic/organic composites. The approach used in this task was two-fold. First, purely inorganic sol-gel processed oxide films of light guiding dimensions were produced and evaluated to determine the waveguide propagation losses. This step allowed the staff of LPT to optimize several processing conditions in an effort to fabricate films with controlled linear index of refraction and thickness. Secondly, the sols of inorganic oxides were doped with organic chromophore(s) in order to introduce second order optical nonlinearity.

In the following sections we present a brief discussion of the requirements imposed on materials for optical waveguides, describe the experimental technique(s) used to evaluate the light propagation losses in a waveguide, and, finally, the experimental results.

Materials Requirements for Nonlinear Waveguide

The material requirements for optical processes in a guided wave geometry are very stringent. They are presented and discussed below.

Control of refractive index

Any material can act as a waveguide providing its index of refraction meets certain criteria. The control over a material's linear refractive index is of great importance since, to function as an optical waveguide, the index of refraction of the guiding medium must be higher than that of the surrounding , cladding and/or substrate. The judicious selection of the linear index of refraction is highly desirable to be able to select specific waveguide modes, confine the guided wave field distribution and to successfully employ various substrates. Such control is also important from the standpoint of optical quality; the refractive index inhomogeneities arising from domain structures should be minimized since they contribute to optical losses.

Control of thickness

In cases where specific wave modes are to be chosen, thickness control is absolutely essential since the effective index of a guided wave mode is directly dependent upon this parameter. Equally important is the ability to control the thickness uniformity which should prevent variations of the mode's effective index; this phenomenon contributes to the overall optical losses.

High optical quality

In order to take advantage of the long interaction length provided by a waveguide geometry, optical losses in a waveguide must be minimized. The optical loss in a waveguide is due to both, absorption and scattering. Processing conditions and structural homogeneity of a material clearly contribute to waveguide losses.

Other material requirements

Among the other factors important waveguide materials are:

(a) high mechanical strength so the waveguide is not easily damaged

(b) excellent environmental stability

(c) high optical damage threshold

(d) the ease with which the material can be cost effectively incorporated into an integrated optical format
(e) film surface smoothness
(f) substrate compatability (for instance their CTES)

D.4.1. Waveguiding characteristics in sol-gel oxide/NPP composite films.

Although there are several methods of coupling light into a thin film waveguide, we have used a prism and holographic grating coupling methods for the planar waveguides. The geometry for the prism coupling experiment is shown in Figure D9a. The substrate covered with a thin sol-gel film is placed on a rotary stage to facilitate smooth adjustment of the laser beam incidence angle. A high refractive index prism ($SrTiO_3$, n_o= 2.396 at 632.8 nm) is brought in physical contact with the film by means of external pressure. The polarized (TE or TM) laser radiation, spatially filtered and collimated in order to match the beam waist with the coupling length at the prism base, is coupled into the waveguide film at the angle Θ. For films supporting more than one mode in each polarization, the computation of refractive indices and the thickness of the waveguide can be performed. To calculate the above quantities, the following waveguide equation has to be solved:

$$2kt\,(n^2 - ß^2)^{-1/2} - 2\Phi_{10} - 2\Phi_{12} = 2m\pi$$

where $ß = n_f \sin\phi$, is the effective refractive index of the waveguide mode m. The angle ϕ is the angle between the guided wave vector and the film normal; t and n are the film thickness and the index of refraction respectively. The quantities Φ_{10} and Φ_{12} are the phase shifts suffered by the wave upon the reflections from the two interfaces : film-cladding and film-substrate. The guided wave effective refractive index, ß, is easily found from the phase matching condition:

$$k \cdot n_p \sin\Theta = k\,ß$$

In the above equation, k is the wave vector of light in air, Θ is the angle between k and the film normal at which the light strikes the prism base and n_p is the prism's index of refraction.

The total waveguide losses are measured by employing a CCD camera to capture and quantitate the scattered light from the waveguide. Figure D8 shows the experimental arrangement used in our measurements.

D.4.2. Experimental results with sol-gel and sol-gel/ NLO composite films

Pure oxide films of optical waveguide dimensions were prepared from a mixture of silicon and titanium alkoxides[1] Various amounts of titanium butoxide were incorporated to control the index of refraction. However, to prevent phase separation of the oxides and a tendency of TiO_2 to crystallize, the concentration of TiO_2 was kept at 50% or lower. The solution of hydrolyzed Si/Ti alkoxides were spin coated on a fused silica substrates at spin speeds between 1300 rpm to 1500 rpm. The films were dried in a vacuum oven at 110 ^{0}C (15 min) prior to densification at 450 ^{0}C for 30 min. The resulting films had a thickness of 0.5 μm or less

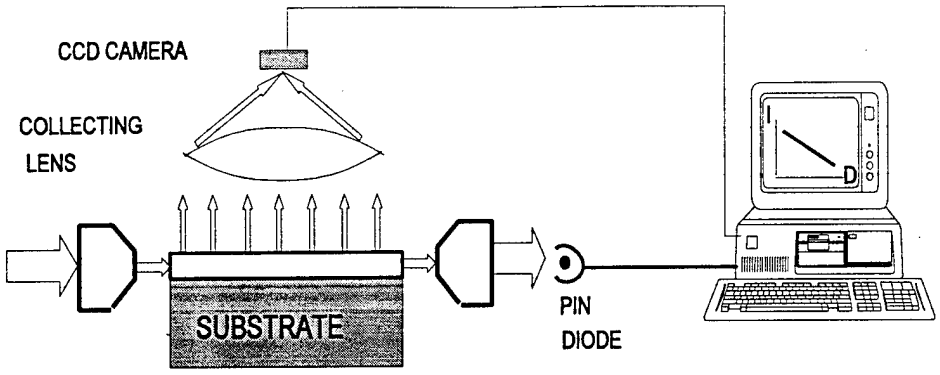

Figure D8 Arrangement for measurement of total waveguide losses.

depending on a spinning speed.

The actual loss measurement was performed by taking a picture of the streak of scattered light using a CCD camera. After correction for the non-linearity of the camera. Summation of all pixels in a column was carried out. A similarly corrected background was subtracted and the intensity of the scattered light is fitted to an exponential decay. Using the assumption that the scattered power is proportional to the guided power, the loss coefficient can be calculated.

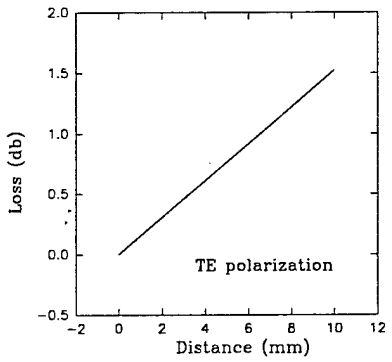

Waveguide propagation loss in SiO_2/GeO_2 sol-gel processed film on BK7 substrate at 632.8 nm.

Figure D9 Waveguide losses in a sol-gel processed SiO_2/ GeO_2 thin film.

Figure D9 displays such a fit to the scattered light intensity observed in sol-gel processed pure oxide cladding and waveguides. Several oxide systems were evaluated for their processability and optical quality (waveguide losses). These included SiO_2/TiO_2, SiO_2/GeO_2 binary oxide systems, and $SiO_2/TiO_2/GeO_2$ tertiary oxide systems. In general, waveguides

fabricated using SiO_2/TiO_2 and $SiO_2/ TiO_2/GeO_2$ exhibited the lowest propagation losses, (1 dB/cm or less as measured at 632.8 nm wavelength).

D.4.3. Loss measurement in planar sol-gel/ NPP waveguides

Sol-gel processed SiO_2,TiO_2 /NPP composite films were prepared by spin coating the solutions of hydrolyzed silca and titania alkoxides doped with NPP onto a fused silica substrates with input and output grating couplers. The optical loss measurements in a sol- gel/NPP films was performed at LPT's laboratories and independently confirmed in the laboratory of our consultant, Prof. G.I. Stegeman. The measurements were performed as a function of the wavelength between 780 nm and 1550 nm before and after heating. The following laser sources were used:

- HeNe laser 632.8 nm
- semiconductor laser 780 nm
- Nd;YAG laser 1064 nm
- Nd;YAG laser 1319 nm
- Er doped Nd;YAG laser 1535 nm

Light was coupled into the waveguide using a grating that was ion milled into the fused silica substrate. The grating period was determined to be 751 nm by measuring the angle of reflection of the first order maximum. In order to achieve efficient coupling of the light into a waveguide, the laser light passed through a telescope to obtain a good collimated beam. Furthermore the beam was focused using a cylindrical lens in order to increase the scattering intensity without disturbing the coupling efficiency.

Typical dependence of the waveguide propagation losses observed at 632.8 nm is presented in Figure D10. Two guided modes were observed at 780 nm. By measuring the two coupling angles of the modes, the thickness, d, and the refractive index, n, of the film were determined to be: 1.460 μm and 1.575, respectively, at λ=780 nm. The results of the loss measurements are summarized in Table D2.

Table D2. Optical loss in sol-gel processed SiO_2, TiO_2/ NPP optical waveguide films at several wavelengths

Propagation loss in sol-gel processed SiO_2, TiO_2/ NPP optical waveguide films					
λ [nm]	632.8	780	1064	1319	1535
Loss (dB/cm)	0.9	< 0.5	< 0.5 dB	3 dB	no loss detected

The losses at 632.8 nm were measured to be 0.9 dB/cm. At 780 nm and 1064 nm, the losses were equal to or smaller than 0.5 dB/cm, which is the lowest measurable loss coefficient using the employed technique and instumentation. At 1319 nm, there is a noticeable increase of the loss. Since the scattering losses should decrease with increasing wavelength, the presence of a small absorption band may explain this sudden increase in the propagation loss. A possible candidate is the presence of hydroxyl groups in the sol-gel matrix. This is justified by the fact

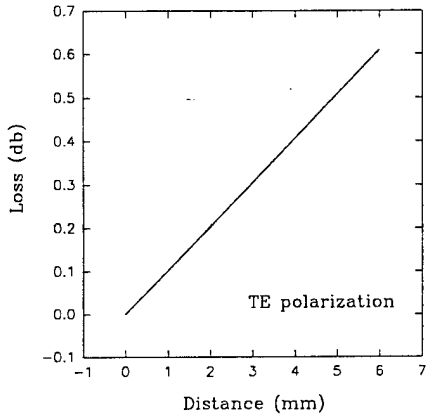

Waveguide propagation loss of SiO_2/NPP sol-gel processed film at 632.8 nm

Figure D10 A typical dependence of the optical losses versus propagation distance in a sol-gel processed SiO_2-TiO_2/ NPP waveguide film.

that the sol-gel films were not processed at high enough temperatures to remove neither water, a byproduct in sol-gel process, nor the unreacted hydroxyls of the silanol species from the oxide matrix. The first overtone vibrations of the O-H group are at 3657 cm^{-1} or 1367 nm (symmetric strech) and at 3756 cm^{-1} or 1330 nm (asymmetric strech). The 1319 nm laser wavelength coincide well with these overtones which supports this proposition. At 1535 nm, no scattered light could be detected, although coupling (in and out) of the laser beam was observed. It is clear that the propagation losses were too small (well below 0.5 dB/cm) to be detected by the instrumentation used in these measurements.

The results presented above clearly indicate that optical quality waveguides can be prepared from sol-gel materials and composites containing NLO chromophores. The process of preparing these waveguides is definitely amenable to integrated optical devices. While many research groups are working on developing NLO polymers for similar applications, it is not clear at this time whether optical losses in these materials are as low as the values presented here. This fact, coupled with the flexibility of the sol-gel process (variable index of refraction, chromophore concentration and replacement, etc.) provides sufficient justification for the use of these materials in preparation of integrated optical structures.

References

1. Zhang, Y., Prasad, P.N., Burzynski, R. *Chem. Mater.,* 1992, *4*, 852

E. ORMOSIL SYSTEMS

In the following section we present a brief introduction to chemically modified organometallic precursors to ceramic materials, commonly called ormosil. This is followed by detailed description of our efforts to synthesize and employ NLO ormosil to produce optical quality films for applications in second-order nonlinear optical processes.

A material that is homogeneous to more exacting standards will be of better optical quality since the domains are less than the wavelength of light (nanometers). Such materials are referred to as *nanocomposites*. Although small crystallites may be too small to scatter light, it is often more preferable to have even finer homogeneity. There are several methods of preparing inorganic-organic materials.

1. Inclusion of Organic Dopants (molecular and polymeric)[1-3]
2. Monomer Infusion with Subsequent Polymerization[4-7]
3. Organofunctional Alkoxysilanes (Ormosil)

A simple example of an ormosil is the compound depicted below.

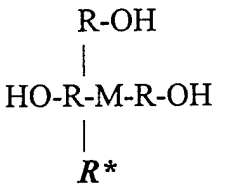

where:

R = 1) CH_2 or 2) CH_2-CH_2

and

R* = an organic functional group introduced to
(1) alter the porosity of the material.
(2) covalently attach another molecule

Note that the typical nondegeneracy of the compound gives the individual molecule multiple functionality. Three of the ligands participate in the hydrolysis and condensation reactions typical of sol-gel processing. The fourth group possesses a different functionality which may be exploited in a number of ways, for instance:

a) modification of the developing network's microstructure.
b) to incorporate a covalently attached compound of interest such as NLO chromophore
c) the establishment of parallel polymeric system.

E.1. Chemistry and Applications of Ormosil

It is indisputable that sol-gel glasses offer exciting opportunities as functional optical materials themselves as well as being host materials for optically active inorganic and organic molecules. Over the past several years many advances have been made in the design and development of optical materials based on sol-gel processing. There are two major approaches to developing sol-gel processed materials containing organic chemicals for optical applications: 1) sol-gel oxide glasses doped with active organic molecules or polymers, and 2) organically modified silicates (ormosil) or ceramics (ceramers). Both approaches have been successful in developing materials with unique properties and having great potential in photonics technology.

Glasses based on modified silicates were used as matrices for second-order optical chromophore *meta*-nitroaniline,[8] laser dyes,[9] and were made into a highly transparent optical

lenses.[10,11] Because ormosil possess organic groups which do not undergo either hydrolysis or the cross-linking condensation reactions, the final material is a molecular level composite comprising of one or more organic functionalities and the silicon-oxygen network. The fact that it is less cross-linked than the usual SiO_2 matrix and contains a polar organic species makes it a suitable environment for trapping sensitive organic and biological molecules.[12] Photochromism and reversed photochromism has been observed in ormosil doped with various spiropyranes.[13-15] An interesting approach to designing electro-optical materials with the desired electro-optical and rheological properties has been presented by encapsulating microdomains of liquid crystals in sol-gel glasses.[16]

The sol-gel process, as defined in this report, involves several chemical processes leading to the final product, ordinarily a porous, and frequently amorphous, oxide glass. The chemical reactions involved: catalytic hydrolysis, polymerization and condensation have already been described in earlier reports. The versatility and uniqueness of sol-gel processing is unmatched by any other material processing technique.[17-24] However, sol-gel processing typically requires large solvent volumes; considerable volume changes during drying pose problem in obtaining good quality crack-free oxide coatings via this approach.

One way to solve these problems is to include organic functionalities into the gel by the use of ormosil. Figure E1 shows a sol-gel process involving the use of a modified silicon alkoxide. The R groups can be chosen to be either inert (alkyl) or organofunctional (epoxy coupling group, vinyl crosslinking group, etc.). Since these groups act as a network modifiers, the type and amount of R strongly affects the material's microstructure and properties. For example, the use of phenyl groups can lead to thermoplastic and soluble polymers.[25]

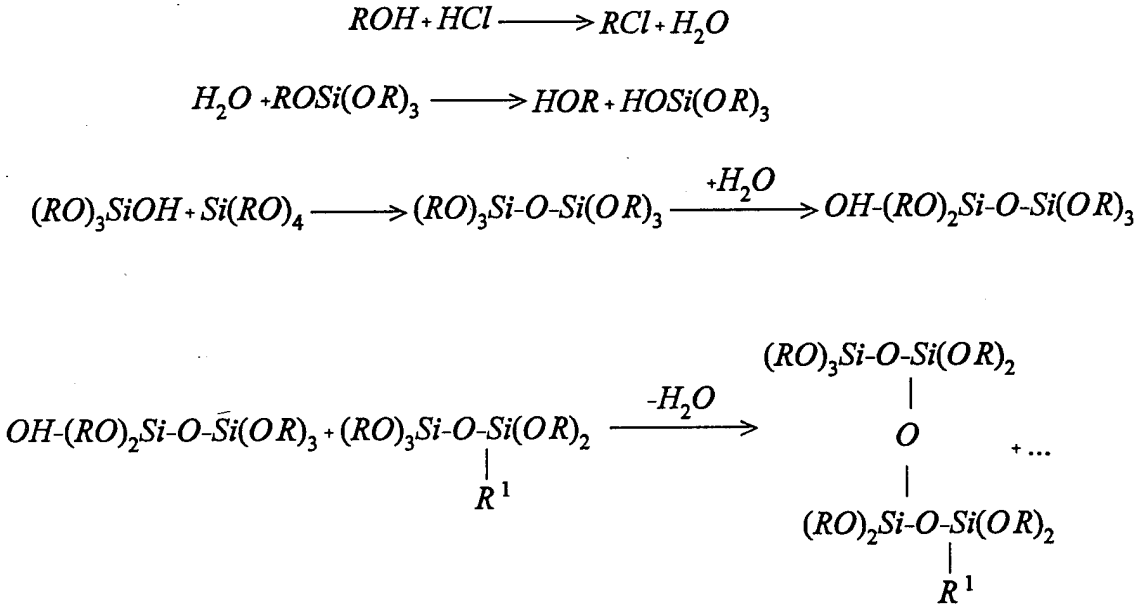

Figure E1. Chemically controlled condensation of Ormosil

Thus, ormosil are hybrid systems in which ceramic components are combined with organic components. The inclusion of particular organic compounds into the developing matrix permits the fine tuning of several physical parameters. Perhaps the most important feature of such a composite network is that the *monomeric units each contain the desired functionality.*

It is important to emphasize that the alkyl trialkoxysilanes hydrolyze and condense at different rates than tetraalkoxy silanes. However, the hydrolysis and condensation rate differences can be controlled by the use of an *in-situ* water generating reaction to avoid H_2O concentration gradients in the system.[25] In this procedure alkyl trialkoxysilane and a small amount of tetralkoxy silane (5-15 mol%) are refluxed first with alcoholic HCl. This *non-hydrolytic* condensation produces low viscosity, stable, partially condensed reactants (precondensates) with a large number of unhydrolyzed ≡SiOR species (see Figure D1). These precondensates can be subsequently further hydrolyzed and condensed by refluxing in aqueous solution of hydrochloric acid to produce viscous liquids suitable for fabricating coatings and monoliths. This chemically controlled condensation (CCC) approach completely avoids phase separation and leads to highly transparent products.

Appendix II presents a detailed description of synthetic routes to ormosil designed at LPT laboratories.

E.1.1. General processing (ormosil only)

(i) Hydrolysis: A mixture of 450 mg 88% formic acid (containing 54 mg of water, 3 equivalent of each triethoxysilane group) and 600 mg freshly dried butanol was added to 606 mg (1 mmol triethoxysilane content) of the ormosil solution. The solution was sonicated for 10 mins. at room temperature and then heated at 60 ^{0}C for 10 mins.

(ii) Film formation: The solution was always cooled to room temperature, filtered through 0.2 μm filter and spincoated at 600 rpm on ITO coated glassplates. The films were dried at 100 ^{0}C under vacuum for 2.5 h.

E.1.2. General fabrication of composite materials (ormosil with sol-gel silica)

A mixture of 450 mg 88% formic acid (containing 54 mg of water, i.e., 3 equivalent for each triethoxysilane group) and 600 mg freshly dried butanol was added to 606 mg (1 mmol Si content) of the DHDO solution. The solution was sonicated for 10 mins. at room temperature, and then heated at 60 ^{0}C for 10 mins. It was cooled to room temperature, and mixed with 184 mg (0.5 mmol Si) of sol-gel silica (TEOS prehydrolyzed either with 1.5 or 4 mole equivalents of water using a mild catalyst). The resulting clear solution was stirred for 5 mins. at room temperature, filtered through a 0.2 μm filter and spincoated at 600 rpm on ITO coated glass plates. The films were dried at 100 ^{0}C under vacuum for 2.5 h.

E.1.3. Application of protective coatings

Two protective coatings were used in an effort to decrease high temperature conductivity (Accuglass 311) and damage to the sample surface caused by high energy ions produced in corona discharge (polymer resins). The Accuglass 311 coatings were applied to the ITO surface while the polymer films were applied over the NLO films.

The coatings were applied as follows: Slides with ITO electrodes were cleaned with detergent, water, acetone, deionized water, followed by isopropanol and dried using compressed dry air. The slides were then spincoated with Accuglass 311 at 3000 rpm for 20 sec., baked at 180 ^{0}C for 60 sec. in air and then cured for 1 hour at 180-425 ^{0}C under nitrogen. The slides were then transferred to a radio frequency glow discharge plasma chamber and treated with 100 watts of RF power under a hydrogen atmosphere (120 torr) for 5 mins in order to modify the coating's surface properties (improved wettability)

Polymer resins were spincoated onto the surface of an NLO ormosil film already deposited on ITO covered glass plates. Among the several polymer resins tested, only polyacrylic acid has been found to be a useful protective coating. It is water and alcohol soluble and it could therefore be removed after poling by soaking the sample in a solvent which doesn't affect the quality and integrity of the NLO film.

E.2. NLO Properties of the Composites

The electric field poling efficiency depends on a large number of parameters such as the poling temperature, poling electric field, environmental humidity and the material itself. The optimal poling conditions vary from one material to another. For this reason the *in situ* poling process has been employed for each sample to determine the best poling conditions. This technique was described in detail in Section B.

It has already been emphasized that during our research on the efficiency of electric field poling, it has been established that the majority of materials suffer surface damage because of the exposure to high kinetic energy ions during the corona discharge.

This observation led us to design a different poling apparatus to be used on materials which have already been established by the *in situ* poling technique. Figure E2 illustrates this design. The main improvement is the introduction of a mesh (set of thin wires) between the corona discharge filament and a sample's surface. A potential of the same polarity as the discharge bias, but much lower in magnitude is applied to the mesh which, then, acts to slow the ionized species (ions). Through the adjustment of bias voltage applied to the screen relative to that needed for corona discharge, an efficient control of the ions' kinetic energy can be achieved without compromising the strength of the poling field across the sample. In this manner, serious surface damage resuting from the bombardment of the sample surface by highly accelerated ions can be prevented. In addition, the apparatus has been designed to pole samples under dry atmosphere of different gases such as nitrogen, argon, helium, etc. This feature provides additional control over poling conditions (and results in the generation of particular ionic species) and a means to avoid highly reactive and oxidizing ions which can easily damage samples.

E.2.1. Poling characteristics and temporal stability

The *in situ* SHG experiments were conducted on all of the material composites described in this report; the ones showing the greatest promise are pure DHDO and DHDO/SiO_2 composite films. For DHDO composites, the second-harmonic signal (monitored as a function of heat treatment with the field applied) typically shows an increase with temperature and reaches a maximum at 135 ^{0}C. Any further temperature increase results in substanial decay of the SHG

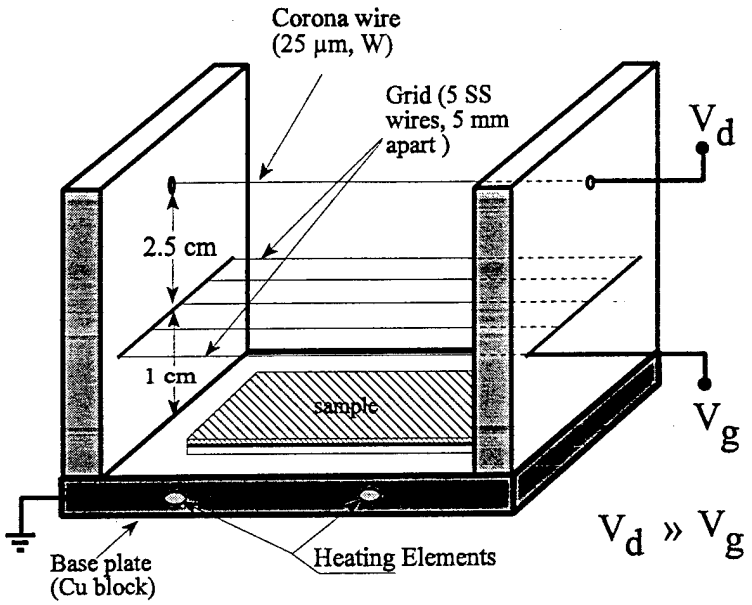

Figure E2 Electric field poling apparatus employing metal grid.

signal. Upon cooling to room temperature, only about 75% of the SHG signal was usually retained. Measurements of temporal stability of the induced alingment revealed that the signal could not be satisfactorly retained. The SHG signal dropped in one month to a level of about 40% of that immediately after the poling. Since such stability is not acceptable for any practical application, we have designed another poling strategy which is more effective for sol-gel and ormosil based composites.

In place of a commonly used temperature "ramp" strategy as presented above, we used a slow ramp/soak approach. This poling scheme involves slow temperature increase to a set point about 30 degrees higher than the preceding one and holding the sample at that temperature for 1 to 2 hours. The hold time at the highest temperature (in majority cases it was 135 ^{0}C to 145 ^{0}C) was usually 3 hours. Longer curing times up to 12 hours as well as higher temperatures were also attempted, but resulted in partial degradation of the composite material. Figure E3 schematically depicts temperature ramp/cure scheme.

Employing ramp/soak poling and curing with NLO ormosil based composite films slightly improved poling efficiency and the stability of the induced noncenrosymmetric structures. The length of the dwell times was determined experimentally and was different for each cure temperature. For example, at temperatures below 100^{0}C, hold/cure times were in general shorter than those above 100^{0}C. It was found that the time needed to reach a plateau of SHG signal was shorter at lower temperatures. This could be related to the proximity to the glass transition tempearture, T_g, and sample conductivity.

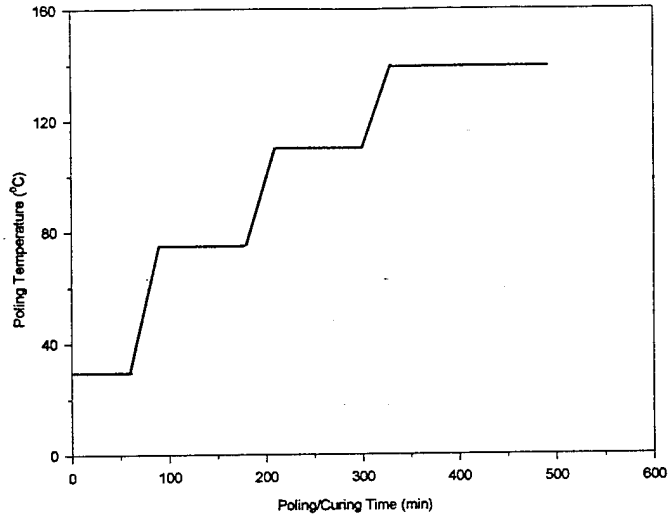

Figure E3 Electic field poling profile used for sol-gel ormosil NLO composites

The observed improvement in poling efficiency on some of our composite materials by using a slow ramp/soak method can be explained by an increased degree of crosslinking between ormosil and silica chains which, effectively, results in an increase of the material's T_g. Thus, each long cure period increases the T_g value, reduces sample's conductivity and increases the electric field strength across the sample. After several ramp/soak steps at higher temperatures further crosslinking and poling becomes more difficult because the matrix is already very stiff. Thus, much longer hold times are needed to reach equilibrium SHG.

In case of mixed ormosil composites, i.e. containing 20 mol% of polymerizable methacryloxy capped ormosil (MMAO) and 80 mol% of DHD ormosil, addopted poling schedule was different than that previously described. First, the films were ramped to 70 - 75°C and kept for a period of about 3 hours. Subsequently, the temperature was raised to 100° and, then to 130°C and was kept at each setting until equilibrium SHG was reached. Next, the temperature was raised in small increments to a maximum temperature of 176°C. After the first 10°C increase, the SHG signal decreased rapidly to about only 10% of its previous value. At this point, the sample was cooled 10°C and kept until the SHG signal recovered to its previous value (i.e. prior to 10 ^{0}C temperature increase). These temperature cycles were continued until the SHG level at the higher temperature setting was the same or higher than that at the lower (by 10°C) temperature setting. This poling scheme resulted in a better thermal stability of the chromophore alignment in a mixed-ormosil composite, as will be shown below.

The temporal stability of the poled structures at ambient conditions has been monitored for an extended period of time by repeatedly measuring the SHG intensity. As can be seen from Figures E4 and E5, these composites show stability of the field induced alignment (at room

temperature) after the poling field has been removed.

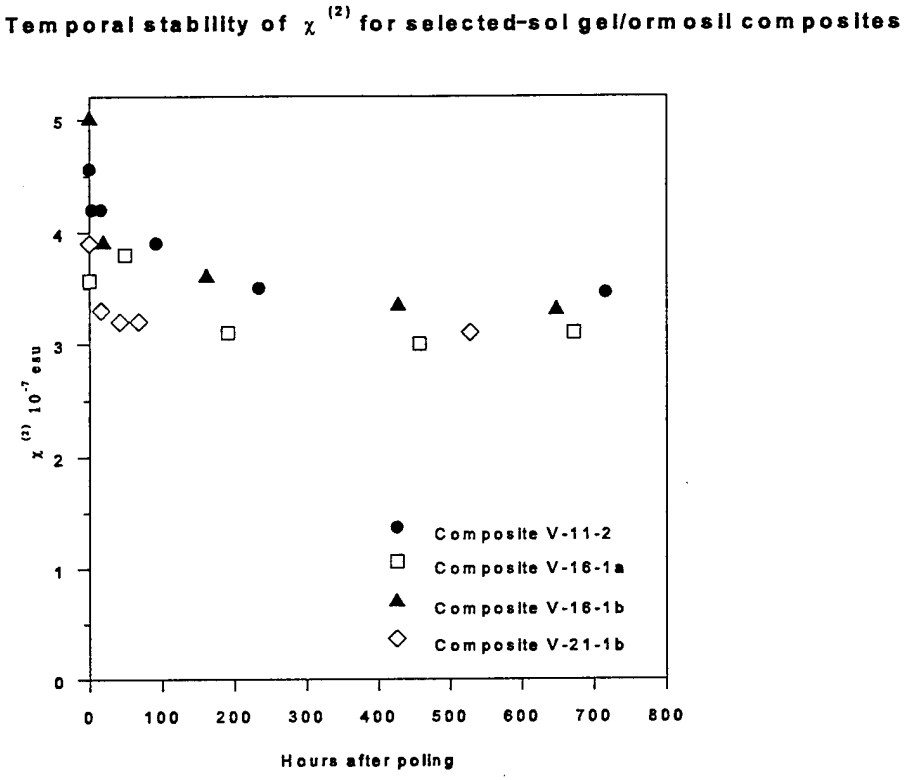

Figure E4 Temporal stability of $\chi^{(2)}$ coefficient for selected sol-gel composites of DHDO ormosil.

E.2.2. Thermal stability

The thermal stability of poled structures was tested dynamically and isothermally. Figure E6 depicts the dynamic thermal stability for two poled ormosil composites: V-16-1 and V-38-2. The stability of the poled structures shown in Figure E6 can be correlated to the molecular structure of the polymers. The rapid decrease of SHG signal at around 70°C for DHDO/SiO_2 composites indicates a low degree of crosslinking and a rather low glass transition temperature. Indeed, a DSC scan revealed an obvious transition around 70°C. This composite was poled under continous thermal ramping with a single cure time of 2 hrs at 135°C. Such a short time may not be sufficient for the composite material to undergo sufficient crosslinking to provide a rigid matrix for poled chromophores, as was discussed above.

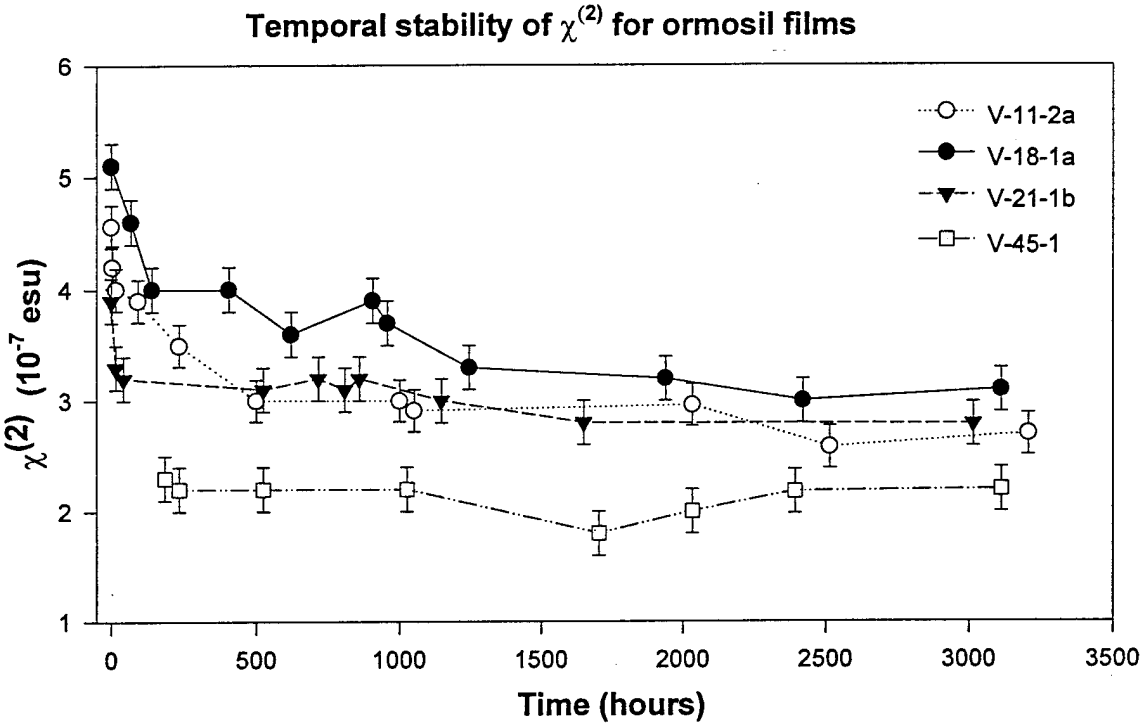

Figure E5 Temporal stability of poled sol-gel processed ormosil films.

Table E1 Molar fraction of chromophore, $\chi^{(2)}$ values of the poled sol-gel ormosil composites composites and chrompophore properties.

NLO Chromophore	Molar fraction in sol-gel composite	$\chi^{(2)}$ (10^{-7} esu)	λ_{MAX} (nm)	Chromoph. dec. temp. (^{0}C)
DHD	0.4	4.7	435	285
NPP	0.3	2.6	393	310
THS	0.2	0.1	383	267

Dynamic thermal stability for pure ormosil composites show somewhat different behavior. The composite was poled using a ramp/soak schedule containing a soak of 3 hrs at the highest temperature (135^{0}C). The total time of the poling process was about 10 hrs. The decrease of the SHG signal does occur over a broader range of temperatures. This feature indicates that more extensive crosslinking between polymer chains took place during the poling process. It has to be emphasised that the ormosil requires longer times to form a highly crosslinked matrix structure because of the lower reactivity of trialkoxysilanes towards hydrolysis as compared to tetraalkoxy silanes. This issue was discussed in detail in our previous annual report.

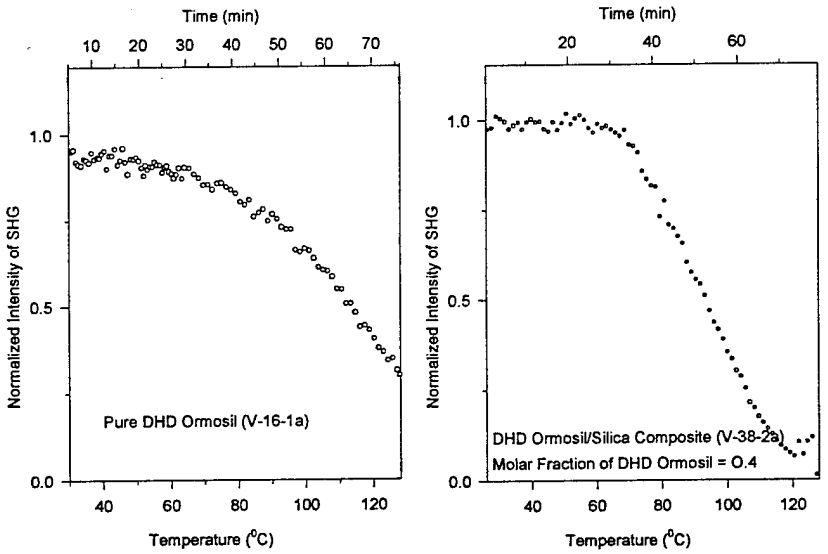

Figure E6 Dynamic thermal stability of $\chi^{(2)}$ coefficient for poled sol-gel/ormosil composite films containing DHD chromophore.

Figure E7 shows the thermal stability of $\chi^{(2)}$ susceptibility for mixed-ormosil (DHDO/MMAO) composite films. The higher temperature (75 ^{0}C) at which an accelerated decrease of the chromophore alignment is observed (as compared to pure DHDO and DHDO/SiO_2 composites) suggests that additional rigidity has been provided to the matrix through a polymerization/crosslinking of methacryloxy groups. Additional feature seen in this figure is that even when the temperature rose above 100 ^{0}C, the SHG value decreased to about 30% of its original value and stabilized at that level (actual $\chi^{(2)}$ susceptibility decreased only 50%). This is another manifestation that careful molecular engineering and judicious choice of ormosil can provide a means to fabricate a very thermally stable NLO material.

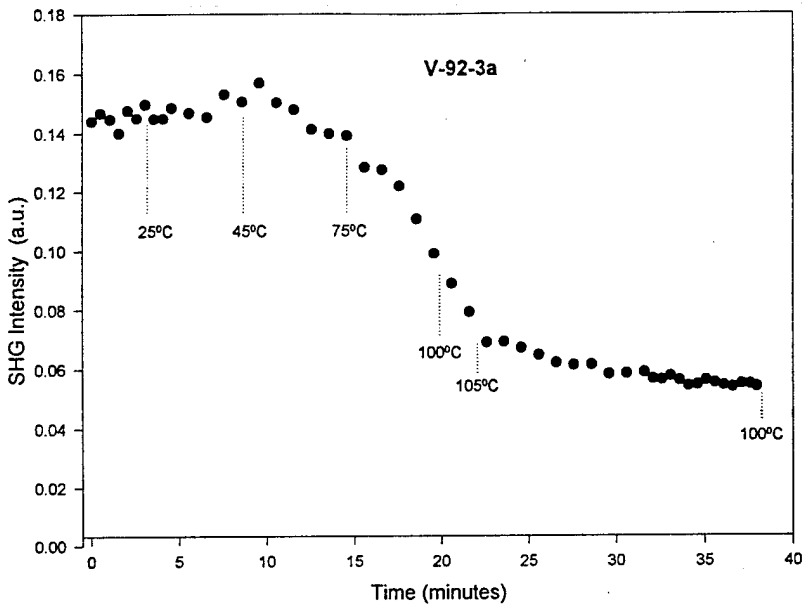

Figure E7 Thermal dynamic stability of $\chi^{(2)}$ susceptibility for DHDO/MMAO ormosil composite

E.3. Waveguide Properties of Sol-Gel Materials

One of the primary requirements of materials developed in this Phase II development effort is the fabrication of low optical loss second order NLO waveguides. We have already disscused that sol-gel materials, being primarily composed of SiO_2, can be made into good optical quality devices. The approach throughout this task was to use ormosil composites in order to increase the materials' homogeneity as well as the number density (in this case molar fraction) of NLO chromophores.

In this task, the staff of LPT focused its work on optimizing several processing conditions in an effort to fabricate films of good optical quality and with controlled thickness. Secondly, the electric field poling process was carefully studied in order to establish conditions which would minimize damage to NLO guiding layers. These efforts were necessary since the material requirements for optical processes in a guided wave geometry are very stringent.

E.3.1. Waveguiding characteristics in sol-gel derived DHD ormosil composite films

Experiments establishing waveguiding quality of ormosil based sol-gel films were accomplished by coupling radiation from an Ar^+ laser pumped tunable Ti-Sapphire laser with the help of $SrTiO_3$ prism coupler. The ormosil films were spincoated on 2 × 1 inch fused silica slides which had been previously overcoated with spinnable glass (Accuglass 311, DuPont) which served as a low index of refraction buffer layer. Several laser wavelengths between 750

nm to 830 nm were used in the experiment. Refractive indices of the composite films varied according to differences in their composition. For example, pure DHDO films had the highest n values which continously decreased as the SiO_2 content increased.

The results show that propagation losses are smaller for longer wavelengths. This trend is expected since the major loss mechanisms at low intensity levels (scattering and linear absorption) are wavelength dependent. Scattering loss scales approximately as λ^{-2} (Rayleigh scattering)[26] and linear absorption follows standard Lambert-Beer law. Thus, for wavelengths further away from electronic transitions, absorption losses become smaller because of a smaller extinction coefficient. A similar trend was observed for the sol-gel composites containing NPP/SiO_2/TiO_2, as discussed in Section D. Optical losses in current waveguides are in a range of 1.6 to 4 $dBcm^{-1}$ (see Figure E8) and are higher than those for NPP composites. However, we expect that with improved processing parameters and fabrication conditions (clean room), propagation losses can be lowered to less than 1 $dBcm^{-1}$ at 800 nm.

Another advantage of DHDO waveguide films is that the content of unreacted hydroxyl groups can potentially be made smaller than in silica sol-gel based doped systems because a molecule of ormosil contains one less alkoxy group. It had been determined by our previous studies and reported a year ago that the presence of hydroxyl groups in the sol-gel matrix is responsible for increased absorption losses at around 1.3 μm. This is because the first overtone vibrations of the O-H group are at 3657 cm^{-1} or 1367 nm (symmetric stretch) and at 3756 cm^{-1} or 1330 nm (asymmetric stretch).

The results presented above clearly indicate that optical quality waveguides can be prepared from ormosil/sol-gel materials and composites containing NLO chromophores. The process of preparing these waveguides is definitely amenable to integrated optical devices. The optical losses in these materials are already acceptably low for practical applications and can likely be substantially improved. This fact, coupled with the flexibility of the sol-gel process

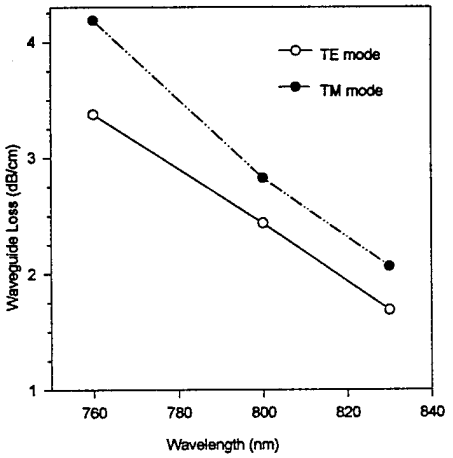

Figure E8 Dispersion of waveguide propagation loss in DHDO composite films for TE and TM modes.

(variable index of refraction, chromophore concentration and replacement, etc.) provides sufficient reason to believe that enhanced materials can be prepared for second-order NLO applications.

REFERENCES

1. Prasad, P.N., Pang, Y., Wung, J.C., Karasz, F.C. (1992). U.S. Patent **5,130,362**
2. Wung, J.C., Pang, Y., Karasz, F.C., Prasad, P.N. (1991). *Polymer*, 32, 605.
3. Kanatzidis, M.G., Wu, C-G., Marcy, H.O., Kannewurt, C.R. (1989) *J. Am. Chem. Soc.*, **111**, 4139.
4. E.J.A Pope; J.D. Mackenzie and W. Yarbrough (1988). In *Ultrastructure Processing of Advanced Ceramics*, eds. J.D. Mackenzie and D.R. Ulrich (Wiley, New York), p.571.
5. E.J.A Pope and J.D. Mackenzie, (1986). Mat. Sci. Research, 20, 187-194.
6. B.I. Lee and L.L.Hench (1986). In *Better Ceramics through Chemistry II*, eds. C.J. Brinker; D.E. Clark and D.R. Ulrich, p.815.
7. B.I. Lee and L.L.Hench, (1987). *Cer. Eng. Sci. Proc.* 8, 685-692.
8. Boulton, J.M., Thompson, J., Fox, H.H., Gorodisher, I., Teowee, G., Calvert, P.D., Uhlmann, D.R.(1990). *Better Ceramics Through Chemistry IV*, Eds., Zelinski, B.J.J., Brinker, C.J., Clark, D.E., Ulrich, D.R. (1990). Mat. Res. Soc. Symp. Proc., Vol. 180, p.987, Pittsburgh.
9. Knobbe, E.T., Bunn, B., Faqua, P.D., Nishida, F., Zink, J. (1992). *Ultrastructure Processing of Advanced Materials*, Eds. Uhlmann, D.R., Ulrich, D.R.. John Wiley & Sons, Inc., New York.
10. Schmidt, H. (1990). *Mater. Res. Symp. Proc.*, 180, 961; Schmidt, H. (1990). *Mat. Res. Symp. Proc.*, 171, 3; Shmidt, H. (1992). *Chemical Processing of Advanced Materials*, Eds., Hench, L.L., Ulrich, D.R.. J. Wiley & Sons, Chapter 64, 727.
11. Schmidt, H. (1988). *Ultrastructure Processing of Advanced Ceramics*, Eds. Mackenzie, J.D., Ulrich, D.R.. Chapter 48, John Wiley & Sons, New York.
12. Avnir, D., Braun, S., Ottolenghgi, M. (1992). *Supermolecular Architecture: Synthetic Control in Thin Films and Solids*, Ed. Bein, T.. ACS Symp. Ser., 499, Chapter 27.
13. Levy, D., Einhorn, S., Avnir, D. (1989). *J. Non-Cryst. Solids*, 113, 137.
14. Levy, D. Avnir, D. (1988). *J. Phys. Chem.*, 92, 4734.
15. Preston, D., Pouxviel, J.-C., Novinson, T., Kaska, W.C., Dunn, B., Zink, J.I. (1990). *J. Phys. Chem.*, 94, 4167.
16. Levy, D., Serna, C.J., Oton, J.M. (1991). *Mat. Lett.*, 10, 470.
17. Altman, J.C., Stone, R.E., Dunn, B., Nishida, F. (1991). *IEEE Photonics Tech. Lett.*, **3**, 189.
18. O'Connel, R.M., Saito, T.T. (1983). *Opt.Eng.*, 22, 393.
19. Gromov, D.A. (1985). *J. Opt. Soc. Am.*, B2, 1028.
20. Avnir, D. Levy, D., Reinsfeld, R. (1984) *J. Phys. Chem.*, 88, 5956.
21. Zink, J.I.Dunn, B. (1991). *J. Matter. Chem.*, 1, 903.
22 Sasaki, H., Kobayashi, Y., Muto, S., Kurokawa, Y. (1990). *J. Am. Ceram. Soc.*, 73, 453.
23. Hench, L.L., West, J.K., Zhu, B.F., Ochoa, R. (1990). *SPIE "Sol-Gel Optics"*, v.1328,

230.
24. He, G.S., Casstevens, M.K., Burzynski, R., Prasad, P.N., unpublished results
25. Schmidt, H., (1989). *J. Non-Cryst. Solids*, 112, 419.
26. P.K. Tien, (1971). *Appl. Opt.*, 10, 2395.

F. CONCLUSIONS

In this Phase II program, Laser Photonics Technology, Inc. demonstrated the preparation of sol-gel processed second-order nonlinear optical composite materials for use in second harmonic generation and electrooptic light modulation processes. This effort involved the syntheses of several second-order NLO chromophores and ormosils, and the development of sol-gel processed composite materials. These materials were processed into waveguiding films having good homogeneity and excellent optical properties. The films also exhibited good mechanical and, in many cases, environmental stability. Characterization of these materials involved the measurements of their absorption profiles, molecular first hyperpolarizabilities, decomposition temperatures, film thicknesses, optical waveguide propagation constants and total propagation losses, refractive indices, *in situ* poling parameters, second-order nonlinear susceptibilities and their temporal and thermal stabilities.

Based on the results of linear and nonlinear optical parameters of various potential candidate sol-gel processed composites, several specially designed and processed materials have been identified as good candidates for application in second-order NLO devices. The ormosil based NLO materials wherein a NLO chromophore(s) is covalently attached to silica network, have provided the best results. This approach permits high NLO concentrations without the potential problem of phase segregation commonly occurring in doped systems. Poling characteristics and studies of temporal stability of the induced $\chi^{(2)}$ functionality in these systems combined with their excellent optical quality (low waveguiding losses) indicate that sol-gel processed ormosils composites can be employed in certain photonic devices utilizing second-order NLO processes. The poled structures showed large and room temperature stable $\chi^{(2)}$ values, reaching a maximum of 5×10^{-7} esu. The thermal stability of the poled films at lower temperatures is satisfactory for some applications but require improvement for several others. This could be accomplished by optimized processing or through the preparation of new composites. The highest temperature at which $\chi^{(2)}$ value did not shown appreciable (more than 10%) decrease was around 75 ^{0}C; the average temperature for the majority of samples was about 45 ^{0}C.

Parallel work accomplished in several laboratories has accomplished the development of polymeric materials with improved thermally stability. An interesting and potentially useful direction might be, the combination of ormosils (alone or with conventional sol-gel precursors) with high T_g polymers. Ormosils can potentially improve optical quality, control refractive indices or even improve thermal stability by introducing an additional network of covalent bonds. However, there are issues of miscibility that clearly need to be contended with.

Preliminary attempts have been made in LPT's laboratories to use Ultradel 9020 and other high T_g polymers used in the electronics industry. It is still too early to say what performance these materials will have. Any clear successes that LPT obtains in this area (now funded by LPT's own resources) will be communicated to the Program Manager.

The presented results indicate the usefulness and applicability of ormosil based composites to integrated optics and photonics devices. Further research, however, needs to be done in order to increase the thermal stabilities of electric field induced noncentrosymmetry while maintaining low optical losses. Finally, the results obtained in this Phase II program strongly suggests that there is

a potential commercial opportunity for nonlinear optical ormosils as materials for second-order processes providing that continued development efforts are focused on the above mentioned material issues.

APPENDIX I

I. SYNTHESES AND MOLECULAR PROPERTIES OF THE SECOND-ORDER NLO CHROMOPHORES:

This section describes the syntheses of the second-order NLO chromophores explored by LPT Phase II. All solvents used in material preparation were purified prior to use.[I-1] All organic reagents were obtained from the Aldrich Chemical Company. Inorganic chemicals and some of the solvents were reagent grade materials from Aldrich Chemical Company, Fisher Chemical Company, and United Chemicals. Extra dry grade Nitrogen and Argon gases were obtained from Union Carbide Corporation, Linde Division and were further dried by passing the gas through a 12 cm x 4 cm column packed with Drierite® (anhydrous calcium sulfate).

All melting points were determined using a Mel-Temp Capillary-Melting-Point Apparatus and were reported in degrees Celcius (°C) (uncorrected). Infrared spectra (IR) were obtained on a Mattson Instruments Alpha Centauri FT Infrared Spectrophotometer. Nuclear Magnetic Resonance (NMR) spectra were recorded on a Varian Gemini-300 300 MHz spectrometer or a Varian VXR-400 400 MHz Spectrometer. All resonances were recorded in δ parts per million (ppm) downfield shift relative to tetramethylsilane. Notations of singlet (s), doublet (d), doublet of doublet (dd), triplet (t), quartet (q) and multiplet (m) are used to designate multiplicity. Coupling constants (J) are recorded in Hz where indicated.

Thermal analyses were done on Shimadzu Differential Scanning Calorimeter DSC-50 and Thermogravimetric Analyzer TGA-50. Combustion analyses were performed by Atlantic Microlab, Inc. P.O. Box 2288, Norcross, Georgia 30091.

The molecular properties of the chromophores are summarized in Table I-1.

I.1. Synthesis of 4-(N,N-Diethylamino)-β-nitrostyrene (DEANST)[I-2]

A mixture of *p*-(N,N-diethylamino)benzaldehyde (**1**) (88.5 g, 0.5 mol), 15 g. ammonium acetate and 500 mL nitromethane was stirred for 8 hours at 100 °C. The mixture was cooled to -20 °C. The precipitated bright red needles were filtered and dried under vacuum. Recrystallization from ethanol yielded 87.8 g (80 %) of the chromophore. M.P. 95 °C.

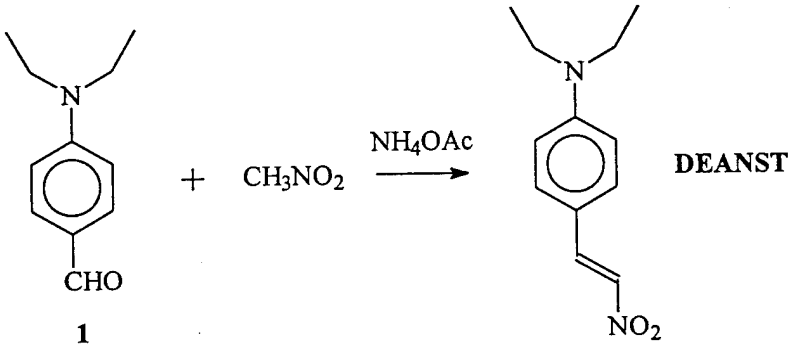

Figure I-1 Synthesis of DEANST

I.2. Synthesis of 4-(N,N-Dihydroxyethylamino)-4'-nitrostilbene (DHD)[I-3]

Pyridine (32 mL, 0.4 mol) was added to a solution of 14.5 g (80 mmol) N-phenyldiethanolamine (**2**) in 100 mL dichloromethane followed by 30 mL (0.32 mol) acetic anhydride. The solution was stirred for 1 h. The reaction was quenched with water and was worked-up using a copper sulfate solution to remove excess pyridine, followed by water and a saturated sodium chloride solution. The solution was dried over anhydrous magnesium sulfate and the solvent was evaporated under reduced pressure to yield 20.8 g (98 %) of acetylated material.

Phosphorus oxychloride (3 mL, 31.5 mmol) was dropwise added to 10 mL (126 mmol) of dry dimethylformamide (DMF) at 0-5 °C under a nitrogen atmosphere. N-Phenyldiacetoxy-ethylamine (8.36 g, 31.5 mmol) was added dropwise to the above reaction mixture. Just after the addition was over, a thick yellow precipitate appeared. The reaction flask was heated at 100 °C for 2 h. After the heating started, the precipitate dissolved and the color of the solution turned brownish. The mixture was then cooled to room temperature and poured in to a 200 mL ice water mixture with vigorous stirring. The solution was neutralized carefully using saturated sodium hydroxide. The precipitate formed was filtered, washed with water and air dried. The solid was dissolved in a minimum amount of methylene chloride and passed through a short silica gel column. The slight yellowish solution obtained after this filtration type chromatography was evaporated to yield 8.86 g (96%) of **3**.

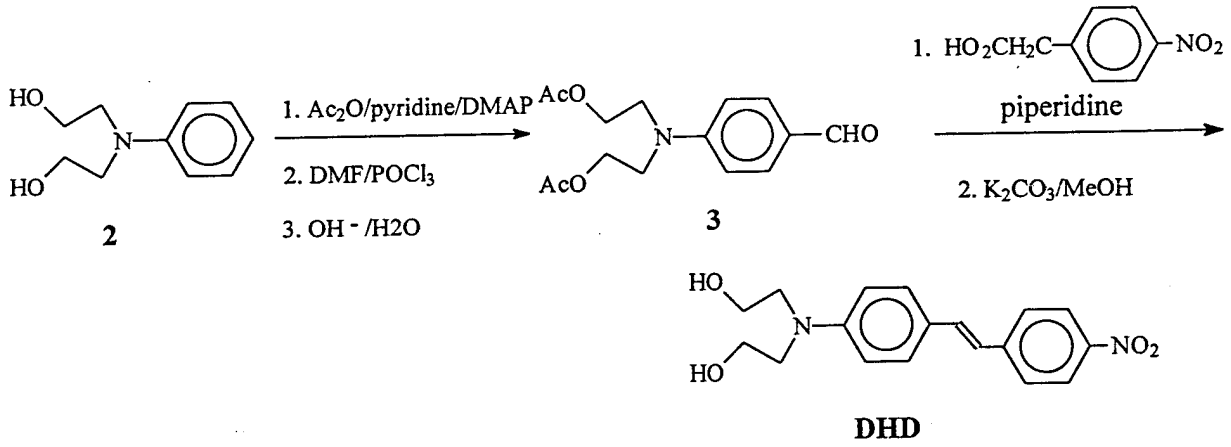

Figure I-2 Synthesis of DHD

Piperidine (2.6 mL, 2.21 g, 26 mmol) was dropwise added to 4.71 g (26 mmol) of 4-nitrophenylacetic acid under nitrogen at room temperature. 4-[N,N-(2,2'-diacetoxyethyl)amino]-benzaldehyde (5.86 g, 20 mmol) was added to this mixture and stirred well. The mixture was then heated at 100 °C for 1 h and at 130 °C for 3 h. It was then cooled to room temperature and 50 mL of methanol was added followed by 5.52 g of potassium carbonate. After stirring for 10 mins., the mixture was filtered and the precipitate was washed with water, air-dried, and recrystallized from toluene (~0.5 L). The yield for shiny chocolate brown colored flakes of DHD

was 2.1 g (32%). M.P. 181-181.5 °C. R_f = 0.11 in 1:1 EtOAc-hexane. ^{1}H-NMR (300 MHz, DMSO-d_6) 8.13, 7.71 (ABq, 4H, J = 8.79 Hz), 7.42, 6.69 (ABq, 4H, J = 8.79 Hz), 7.38, 7.05 (ABq, 4H, J = 16 Hz), 4.78 (t, 1H), 3.51 (t, 4H), 3.45 (t, 4H).

I.3. Synthesis of N-(4-Nitrophenyl)-(L)-prolinol (NPP)[I-4]

A solution of (S)-(+)-2-pyrrolidinemethanol (**4**) (20.25g, 0.2 mol) in 20 mL of freshly dried dimethyl sulfoxide was mixed with 21.2 mL 1-Fluoro-4-nitrobenzene (**5**) (28.2 g, 0.2 mol) and 27.6 g. potassium carbonate (0.2 mol). The contents became orange after mixing and there was a vigorous evolution of gas for about 5 mins. The mixture was heated at 60 °C for 24 h., then cooled and was dropwise added to a 500 mL ice water mixture with vigorous stirring. The solid yellow precipitate was filtered, dried and recrystallized from toluene. Yield: 38.3 g (86 %). M.P. 118 °C.

IR (KBr) 3460, 1600, 1485 cm^{-1};
^{1}H-NMR (300 MHz, $CDCl_3$) δ 8.02, 6.53 (AB_q, J=7.5, 4H), 3.98 (m, 1H), 3.55-3.72 (m, 2H), 3.52 (m, 1H), 2.05 (m, 2H) ppm;
^{13}C-NMR (300 MHz, $CDCl_3$) δ 152.75, 137.35, 126.84, 111.57, 62.94, 60.66, 49.22, 28.60, 23.39 ppm.

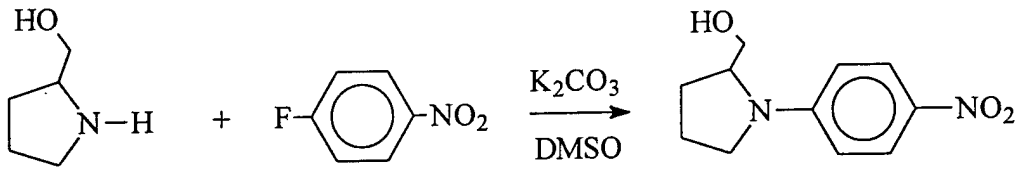

4 **5** **NPP**

Figure I-3 Synthesis of NPP

I.4. Synthesis of 2-(Dimethylamino)-6-propionylnaphthalene (PRODAN):[I-5]

In a 3 neck 200 mL round bottom flask, under argon atmosphere, at room temperature, equipped with gas inlet tube, 3.5 g (77 mmol, 4.3 equiv.) of gaseous dimethylamine was dissolved in a mixture of 19 mL hexamethylphosphoramide and 20 mL benzene. 500 mg (71 mmol) of lithium ribbon was added to the mixture and stirred for 2 hours until all the lithium dissolved. To the mixture was added 3.85 g (18 mmol) of 2-methoxy-6-propionylnaphthalene (PROMEN) (**6**) at once. The progress of the reaction was checked using tlc. The mixture was stirred for 10 h. under argon. R_f = 0.47 in 1:5 THF-hexane, M.P. 137 °C, ^{1}H-NMR ($CDCl_3$, 300 MHz) δ 8.30 (s, 1H), 7.9 (dd, 1H), 7.77, 7.61 (AB_q, J = 8.5 Hz, 2H), 7.14 (dd, 1H), 3.05 (m, 8H), 1.23 (t, 3H) ppm.

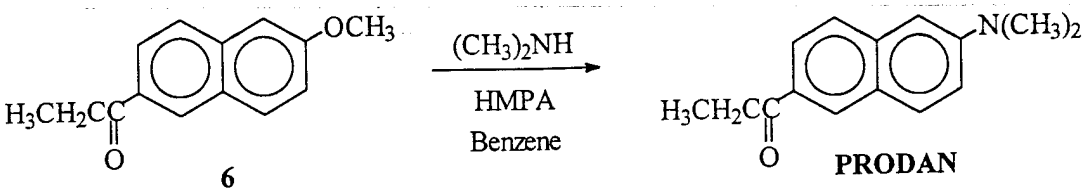

Figure I-4 Synthesis of PRODAN

I.5. Synthesis of 4-Diethanolamino-4'-(6-hydroxyhexylsulfinyl)stilbene (THS):

6-Hydroxyhexyl-*p*-tolyl sulfide (8): To 500 mL ethyl alcohol under nitrogen at room temperature was slowly dissolved 13 g (0.562 mol) of sodium globules. The solution was brought to 0-5 °C and 63.5 g (0.511 mol) of thiocresol (**7**) was added followed by 80 g (0.562 mol) of 6-chloro-1-hexanol (96%). The temperature of the mixture was raised and was refluxed for 10 h. After cooling the reaction mixture, it was filtered and the solvent was evaporated off. After filtering through a short silica gel column using methylene chloride as the solvent, the crude white material was recrystallized from hexane to yield 108 g. (95%) of **8**.

6-Acetoxyhexyl-*p*-tolylsulfide (9): In an 1 liter round bottom flask, 77.5 g (0.346 mol) **8** was dissolved in 500 mL of dry methylene chloride and 70.6 g (65 mL, 0.692 mol) of acetic anhydride was added to it followed by 55 g (56 mL, 0.692 mol) of pyridine. A catalytic amount (4.2 g, 34.6 mmol) of N,N-dimethylaminopyridine (DMAP) was added to the clear solution and it was stirred for 1 h. The reaction was quenched with the addition of water and the methylene chloride layer was washed with 10 % aqueous solution of cupric sulfate, until all the pyridine was removed (checked by tlc), followed by water and saturated sodium chloride solution. The organic layer was dried over anhydrous magnesium sulfate and was evaporated to give a clear oil of **9**.

6-Acetoxyhexyl-p-tolylsulfinate (10): In an 1 liter round bottom flask, 92 g (0.346 mol) of the sulfide **9** was dissolved in 350 mL glacial acetic acid and heated to reflux. Hydrogen peroxide (80 mL, 0.692 mol) was added dropwise from the top of the reflux condenser at the rate just to keep the solution boiling under control. The solution was refluxed for 2 h. after the total addition of all the hydrogen peroxide and then the acetic acid was distilled off. The clear liquid was washed with water and saturated sodium chloride solution and was dried over anhydrous magnesium sulfate to yield 100 g of **10**. ^{1}H-NMR ($CDCl_3$, 300 MHz) δ 7.76, 7.34 (AB_q, J = 8 Hz, 4H), 4.00 (t, 2H), 3.05 (t, 2H), 2.45 (s, 3H), 2.02 (s, 3H), 1.69 (m, 2H), 1.56 (m, 2H), 1.34 (m, 4H) ppm.

6-Acetoxyhexylsulfinyl benzyl bromide (11): In an 1 liter round bottom flask equipped with a straight condenser, 100 g (0.336 mol) of sulfinate **10** was dissolved in 300 mL of dry carbon tetrachloride. The solution was brought to reflux and a mixture of 59.7g (0.336 mol) N-bromosuccinimide and 8.13 g (33.6 mmol) benzoyl peroxide was added portionwise over a time

period of 1 h. The progress of the reaction could be followed since the product, succinimide, is lighter than the solvent. After 10 mins. of refluxing, the mixture was cooled rapidly to 0-5 °C and was filtered to remove succinimide. The filtrate was left in the refrigerator for 2 days with occasional scratching on the side of the flask. The crystals formed were filtered and dried under vacuum to yield 88.17g (70%) of pure white crystals of **11**. ^{1}H-NMR ($CDCl_3$, 300 MHz) δ 7.88, 7.58 (ABq, J = 8 Hz, 4H), 4.505 (s, 2H), 4.01 (t, 2H), 3.09 (t, 2H), 2.02 (s, 3H), 1.75 (m, 2H), 1.60 (m, 2H), 1.37 (m, 4H) ppm.

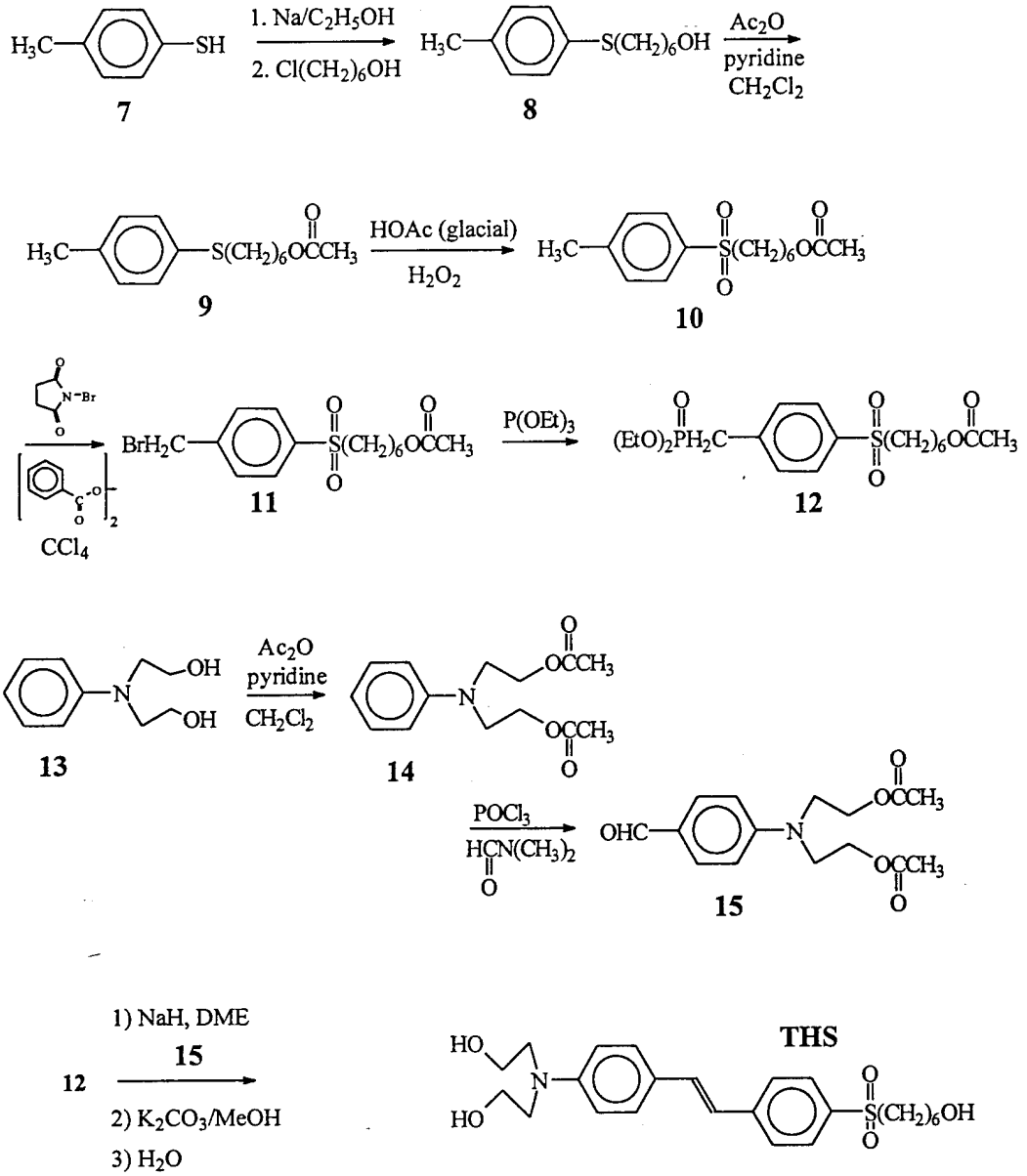

Figure I-5 Synthesis of THS

6-Acetoxyhexylsulfinyl benzyl phosphonate (12): To 20.73 g (55 mmol) of melted bromide **5**, at 100 °C, under nitrogen, 13.7 g (14.13 mL, 82.5 mmol) of triethyl phosphite was dropwise added over 20 minutes. The temperature rose to 120 °C and maintained for 2 more hours. Excess triethyl phosphite was distilled off and the thick colorless liquid was used for the next step without further purification.

N-Phenyldiacetoxyethylamine (1-4): In an 1 liter round bottom flask 45.25 g (0.25 mol) of **13** was dissolved in 500 mL dry methylene chloride and 102 g (92 mL, 1.0 mol) acetic anhydride was added to it followed by 49 g (50 mL, 0.625 mol) pyridine. A catalytic amount (3.0 g, 25 mmol) of N,N-dimethylaminopyridine (DMAP) was added to the clear solution and it was stirred for 1 h. The reaction was quenched with the addition of water and the methylene chloride layer was washed with a 10 % aqueous solution of cupric sulfate, until all the pyridine was removed (checked by tlc), followed by water and saturated sodium chloride solution. The organic layer was dried over anhydrous magnesium sulfate and was evaporated to give 63.6 g (96 %) of a clear oil (**14**).

4-(2,2'-Diacetoxyethylamino)benzaldehyde (15): To 75 mL DMF at 5 °C under nitrogen was dropwise added 23 mL phosphorus oxychloride. To this light brown colored solution, 63.3 g (0.239 mol) of the acetate **14** was added. Towards the end of the addition, the cooling bath was removed due to the difficulty in stirring the thick yellow precipitate. This slurry was then heated for 1.5 h, cooled to room temperature and poured into 400 mL of ice cold water. A cooled solution of 40 g (1 mol) sodium hydroxide in a minimum amount of water was dropwise added to neutralize the brown solution. The solution was filtered and washed with water. The crude material was dried under vacuum, dissolved in methylene chloride and filtered through a silica gel column with 1:2 ethyl acetate-hexane mixture. Total yield after evaporation was 54.5 g (78 %). M.P. 54-6 °C. ^{1}H-NMR ($CDCl_3$, 300 MHz) δ 9.72 (s, 1H), 7.71, 6.78 (AB_q, J = 8.5, 4H) 4.26 (t, 4H), 3.7 (t, 4H), 2.01 (s, 6H) ppm.

4-Diethanolamino-4'-(6-hydroxyhexylsulfinyl)stilbene (THS): To 1.2 g (30 mmol) sodium hydride (60 % dispersion in mineral oil) (washed with 3 x 5 mL DME), a solution of 13.0 g (30 mmol) of phosphonate **12** in dry DME was added followed by 8.79 g (30 mmol) aldehyde **15**. The mixture was refluxed for 2 days. The reaction mixture was cooled and quenched with water. The excess solvent was removed under vacuum and was filtered through silica gel using ethyl acetate as solvent. The solvent was evaporated and the sticky yellow material was dissolved in 500 mL methanol followed by addition of 12.4 g (90 mmol) of potassium carbonate. The mixture was stirred for 2 h. and excess potassium carbonate was filtered off. Two thirds of the solvent was evaporated under vacuum and the rest of the thick solution was poured into an ice water mixture. The yellow precipitate was collected by filtration and recrystallized from chloroform to yield 1.8 g (13 %) of **THS**. M.P. 120 °C. ^{1}H-NMR ($CDCl_3$, 300 MHz) δ 7.73 (q, 2H), 7.41, 6.67 (AB_q, J = 8.5, 4H), 7.30, 7.00 (AB_q, J = 8.5, 4H), 4.76 (t, 2-OH), 4.30 (t, 1-OH), 3.50 (m, 4H), 3.42 (m, 4H), 3.25 (m, 4H), 1.50 (m, 2H), 1.25 (m, 6H) ppm.

Table I-1: Molecular weights (MW), melting points (MP), absorption maxima (λmax), first nonlinear hyperpolarizabilities (β), and the decomposition temperatures of the chromophores.

Molecular Structure	MW	MP (°C)	λmax (nm)	β ($\times 10^{30}$ esu)	Decomp. Temp.(°C)
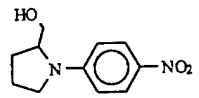 NPP	222	116	393	86.2 ($CHCl_3$)	310
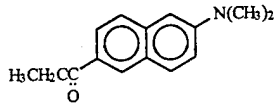 PRODAN	227	137	355 ($CHCl_3$)	39 ($CHCl_3$)	290
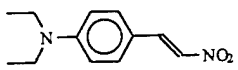 DEANST	220	95	432 ($CHCl_3$)	222 ($CHCl_3$)	240
DHD 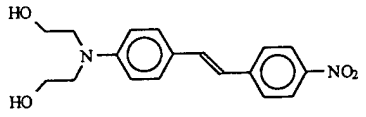	328	181	430	350 (est)	297
THS 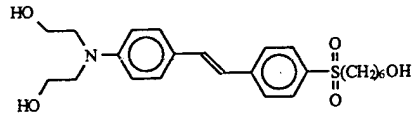	447	120	383	120 (est)	267

References:

I-1. D.D. Perrin, W.L.F. Armarego, and D.R. Perrin, "*Purification of Laboratory Chemicals*," Pergamon Press, New York, 1980.

I-2. T. Kurihara, H. Kanbara, H. Kobayashi, K. Kubodera, S. Matsumoto, and T. Kaino, *Optics Comm.* **84**, 149 (1991).

I-3. R.D. DeMartino, *U.S. Patent* **4,757,130** (1988)

I-4. J. Zyss, J. F. Nicoud, and M. Coquillay, *J. Chem. Phys.*, **81**, 4160 (1984).

I-5. G. Weber and F. J. Farris, *Biochemistry*, **18**, 3075 (1979).

APPENDIX II

II. SYNTHESIS AND PROCESSING OF NLO ORMOSILS

In the following paragraphs we describe in detail our synthetic efforts to produce stable chromophore substituted ormosils. The approach was to modify commercially available ormosils by covalently attaching NLO chromophores to the ormosil's alkyl chain terminated with reactive functional groups, such as chlorine atoms or isocyanate groups.

II.1. Formation of the Ether Linkage for the Formation of Ormosils:

The first step in LPT's efforts to prepare chromophore substituted ormosils is to prepare an ether linkage between the chromophore and the alkoxide. The usual procedure for the formation of ether linkages is to heat an alcohol and a chloro compound in the presence of some base.[II-1] The bases used for our reaction were (a) diisopropylethylamine and (b) lithium diisopropylamide. The progress of the reactions was quickly checked with thin layer chromatography; the crude reaction mixture showed up at the same R_f value (0.45 in 1:1 ethyl acetate-hexane) as the starting NPP.

The 3-iodopropyltrimethoxysilane [$I(CH_2)_3Si(OMe)_3$] is more reactive than the chloro substituted compound for the substitution reaction, we prepared this iodo derivative and proceeded with the etherification reaction. However, the hydrolysis of the C-O-C bond is also fast in the presence of a base, which again hindered the forward reaction, as in the case of the chloro derivative.

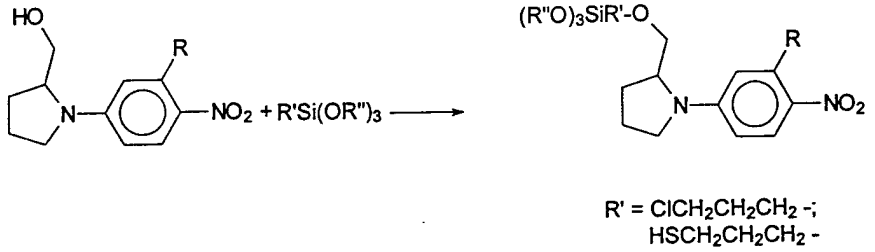

Figure II-1 Example of the synthetic approach to chromophore substituted ormosils

Following these attempts, it was decided to use a higher temperature to facilitate the forward reaction instead of a base. A mixture of 1.78 g (8 mmol) NPP and 5 mL (27 mmol, 3.4 equiv.) 3-chloropropyl trimethoxysilane was heated at 170 °C for 16 h. (overnight). The mixture was cooled to room temperature and chromatographed on silica gel. The pure ormosil obtained was checked with ^{1}H-NMR and found to be consistent with our expectations.

II.1.1 Hydrolysis of the ormosils (use of acids or bases):

The hydrolysis of the trimethoxysilyl group was attempted in dilute acidic or basic media. Unfortunately, the C-O-C ether linkage is more susceptible to hydrolysis than the C-O-Si bond. The hydrolysis rate for the three methoxy linkages attached to silicon become slower after each step, which slows down the gelation procedure.[II-2]

II.1.2. Use of titania:

Partially prehydrolyzed titanium alkoxide (using the nonhydrolitic approach presented above) was mixed with the reaction mixture before starting the reaction. This step was undertaken in order to facilitate a faster rate of hydrolysis and condensation of the ormosil as depicted in Figure II-2.

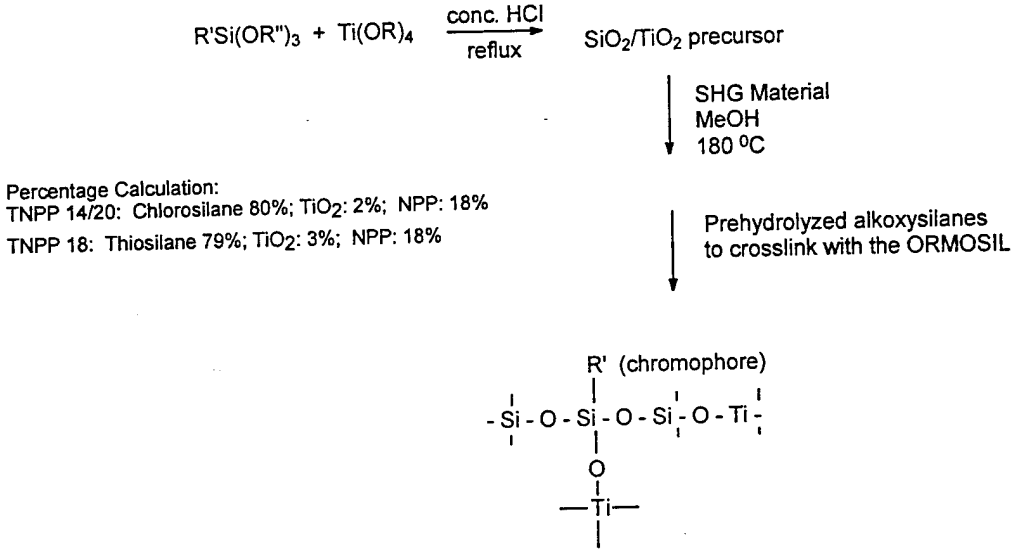

Figure II-2 Use of titanium alkoxide in the preparation of NLO chromophore substituted ormosil

II.2. Formation of the Carbamate Linkage for the Formation of Ormosil:

II.2.1. Preparation of O,O'-[2-(4-Ethylamino-4'-nitrostilbenyl)]-bis-(N,N'-[3-(triethoxysilylpropyl)]carbamate) (DHDO): In a 50 mL flask, a mixture of 1.31 g (4 mmol) DHD, 2.96 g (12 mmol, 3 equiv.) 3-(triethoxysilyl)propyl isocyanate, 2 mL chlorobenzene, and 6 drops of HMPA (hexamethylphosphoramide) were mixed together and heated for 24 hours at 110 °C. Chlorobenzene was distilled off under vacuum. The remaining dark red colored semi-solid was diluted with 3 mL freshly dried isopropanol and left sealed under nitrogen until further use.

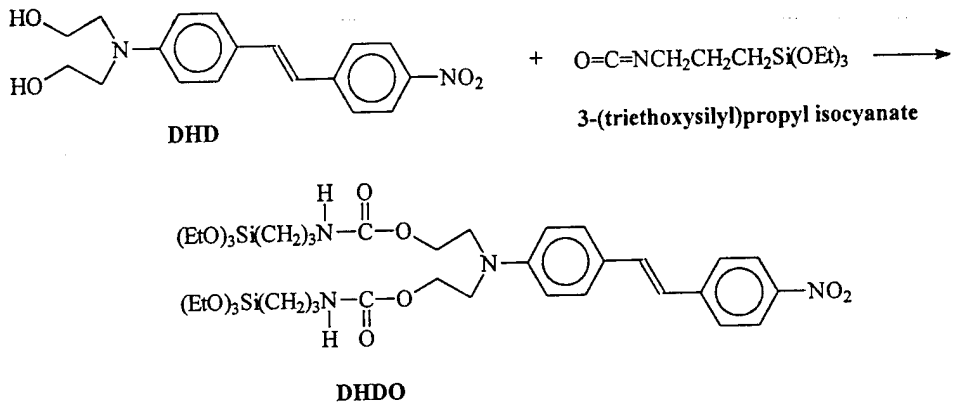

Figure II-3 Chemical Route to DHDO

II.2.2. Preparation of O,O'O''-[2-(4-Ethylamino-(4'-(6-hexylsulfinyl))]-tris-(N,N',N''-[3-triethoxysilylpropyl]carbamate) (THSO):

THSO was synthesized using procedures depicted in Figure II-4. THS (223 mg, 0.5 mmol) and 3-(triethoxysilyl)propyl isocyanate (371 mg, 1.5 mmol) were mixed with 1 mL chlorobenzene and heated for 24 hours at 110 °C under nitrogen. The chlorobenzene was distilled off and 1 mL isopropanol was added to dissolve the yellow semi-solid.

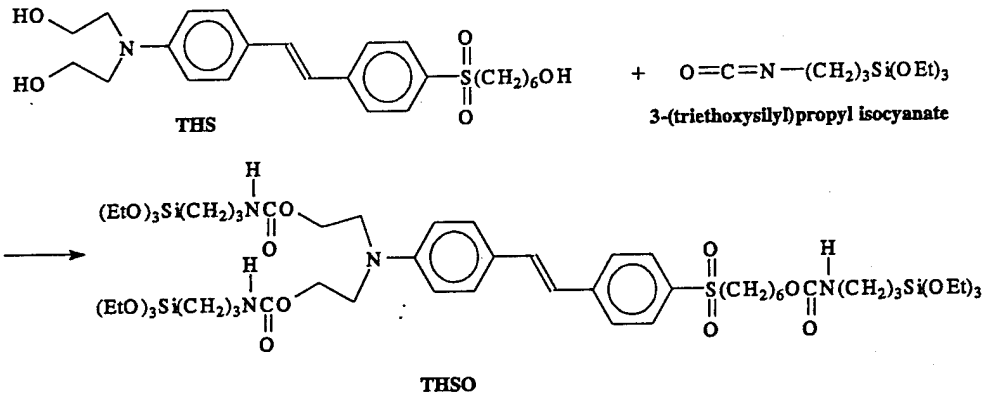

Figure II-4 Synthesis of an NLO ormosil (THSO) containing THS

References:

II-1. E.J. Corey, J.L. Gras, and P. Ulrich, *Tetrahedron Lett.* 809 (1976).

II-2. J. Kim, J. L. Plawsky, E. van Wagenen, G.M. Korenowski, *Chem. Mater.* to be published.

APPENDIX III

III. PREPARATION AND PROPERTIES OF NLO COMPOSITE FILMS

This section provides details of LPT's efforts in processing and preparing ormosil based films and composites. The chromophores containing a reactive functionality were covalently attached to other ormosils to provide the solubility and more importantly, the stability of the SHG signal. The preparation of these chromophore containing ormosils were described in Appendix II. This section now details the film formation of these NLO composites. In order to improve the SHG signal stability of the chromophore films and to simplify the hydrolysis procedure, the conditions of film formation were systematically changed. In the following description, numeric codes have been used for easy indentification of each composite material. NLO properties, thicknesses and $\chi^{(2)}$ stabilities are listed for the corresponding film.

III.1. Films Formed From Ormosils Derived From NPP and Related Chromophores

(a) Hydrolysis of tetraalkoxysilanes

To hydrolyze alkoxysilanes, 2.0 g TMOS was mixed with a mild catalyst and, while stirring vigorously, 500 mg water was added to this mixture.

(b) Preparation NPP composite films

TNPP 14/20: A Ti-SiCl stock solution was prepared: a mixture of 1.36 g $Ti(OBu)_4$ (4 mmol), 4 g 3-chloropropyl trimethoxysilane (20 mmol), 2 mL MeOH and 100 mg concentrated HCl was taken and refluxed for 0.5 h., 750 mg 3-chloropropyl trimethoxysilane was added to 400 mg of the stock solution and heated for 1 h at 80-110 °C. After cooling to 50 °C, 222 mg NPP was added to this mixture and slowly heated to 180 °C for 5 minutes. Then the solution was cooled to room temperature and 800 mg cyclopentanone was added followed by 250 mg prehydrolyzed silica (2 h old). The solution was filtered through a 0.45 μm filter. Films were spin coated on an ITO coated substrate at 550 rpm and other films were hand-cast on ITO. Both film types were dried in the oven at 60 °C for 3 days.

These films could be formed with relative ease in a wide range of thicknesses ranging from a few to several tens of micrometers. They could be effectively poled at relatively low temperatures using the corona discharge technique and gave a good signal in the SHG measurements. However, the induced alignment was not stable evidenced by a fast disapearance of SHG signal at room temperature. Attempts to align chromophores at higher temperatures, *i.e.* above 120 °C, did not result in better stability of the induced noncentrosymmetric order.

THNP: A stock solution was prepared as follows: 6.8 g [20 mmol] titanium butoxide, 8g (40 mmol) 3-chlorotrimethoxysilane, 10 mL MeOH, and 240 mg concentrated HCl were refluxed for 0.5 h. 440 mg Chlorosilane (more than a month old), 1 g MeOH and 400 mg HNPP were added to 250 mg of the stock solution and heated for 1 h at 180 °C. It was cooled to RT and 526 mg of mix prehydrolyzed silica was added. 450 mg cyclopentanone was added to 1 g of this mixture. The solution was filtered and films were prepared by (a) spincoating on ITO at 600 rpm, (b) handcast, or (c) spincoating at 300 rpm for 4-5 sec. and were subsequently heated at 140 °C. Films (a) and (c) were coated with resin and poled at 190 °C for 10 mins. The films turned black indicating nonspecific decomposition.

TNPP18: To 800 mg of stock solution (681 mg [2 mmol] $Ti(OBu)_4$, 3.93 g [20 mmol] 3-mercaptopropyltrimethoxysilane, 100 mg conc. HCl and 2 g MeOH were mixed and refluxed for 0.5 h), 111 mg NPP were added and heated to 170 °C for 5 mins. It was slowly cooled to room temperature and 200 mg hydrolyzed tetraalkoxysilanes was added (one day old). It was filtered through a 1 μm filter and the solutiuon was spincoated on ITO at 300 rpm.

TBNP25: To 800 mg of stock solution (a mixture of 380 mg [2.2 mmol] Ti-butoxide, 2.74 g trimethoxybenzylethylsilane and 3 drops conc. HCl was refluxed for 0.5 h), 222 mg NPP was added and heated to 140 °C. 800 mg cyclopentanone was added to this and filtered through 1 μm filter followed by the addition of 100 mg hydrolyzed tetraalkoxysilane. The final material was spincoated at 550 rpm on ITO coated substrate and heated at 60 °C for 2 h and then at 80 °C for 2 days.

THNP20: To 400 mg stock solution (a mixture of 1.36 g $Ti(OBu)_4$ (4 mmol), 4 g 3-chloropropyl trimethoxysilane (20 mmol), 2 mL MeOH and 100 mg conc. Hcl) was taken and refluxed for 0.5 h.), 750 mg 3-chloropropyl trimethoxysilane was added and heated for 1 h at 110 °C. The mixture was cooled to room temperature 238 mg HNPP was added. It was then heated slowly to 183 °C and was kept there for 10 mins. It was slowly cooled to room temperature. 800 mg cyclopentanone was added followed by 160 mg hydrolyzed tetraalkoxysilane (1 h old). The thick solution was filtered through a 0.45 μm filter and spincoated at 550 rpm on ITO coated substrate and baked at 60 °C.

Films made of the last four ormosil-NLO chromophore composites did not show the expected increase in $\chi^{(2)}$ value. However, the approach presented here has not exhausted all methods all prospects of producing NLO ormosils which exhibit large optical nonlinearities and thermal stabilities. The likelihood of achieving this goal is very feasible. The main motivation of pursuing this approach is that higher concentrations of the chromophore species can be incorporated into a sol-gel matrix without concern of potential phase segregation (precipitation, crystallization, etc.). Furthermore, the formation of a strong covalent bond between the chromophore and the ormosil matrix is possible and has been documented by Jeng et al.[III-1,III-2] Our continued efforts in this area includes the synthesis of an ormosil with a NLO chromophore attached to it by a strong bond such as C-C. This prevents potential dissociation of the covalent linkage between the chromophore and the ormosil since the C-C bond does not hydrolyze, unlike the linkages of the C-O-C type, in conditions required to hydrolyze the alkoxy groups.

III.2. Preparation of DHD Composite Films

IV-99-1: To a mixture of DHDO, isopropanol, partially hydrolyzed silica (Si content 1:1), water was added for full hydrolysis, *i.e.*, 3 molar equivalent for each $Si(OEt)_3$ and 4 molar equivalent for each $Si(OEt)_4$. The mixture was heated at 60 °C and spincoated. The films were heated for 15 mins. at 100 °C.

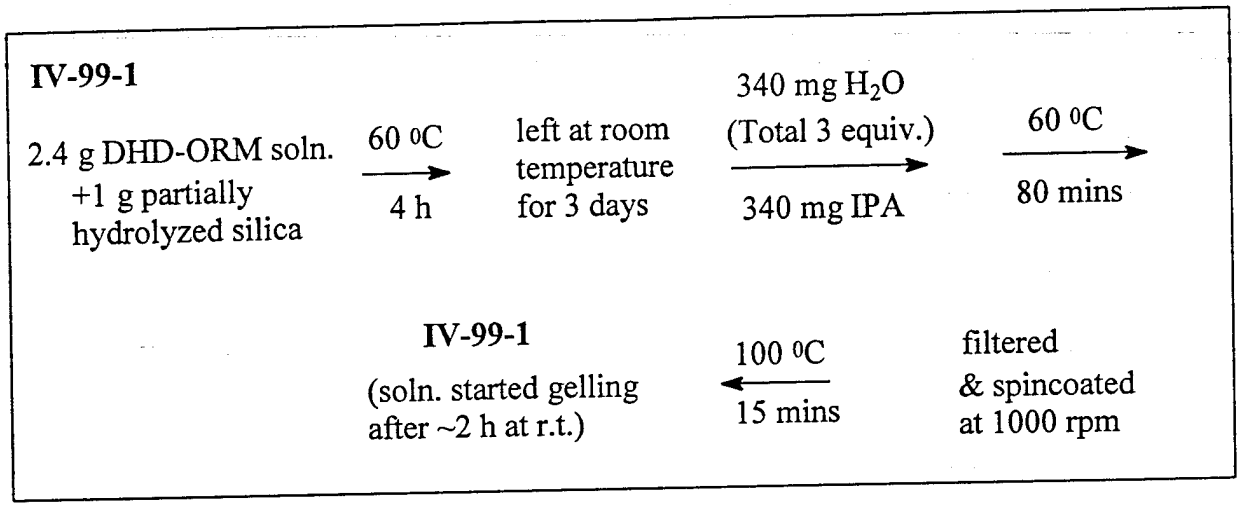

Figure III-1 Preparation of IV-99-1 sol-gel composite

V-3-3: This procedure is the same as IV-99-1, except cyclopentanone and isopropanol were added to prevent gelling. Films were much thinner than IV-99-1.

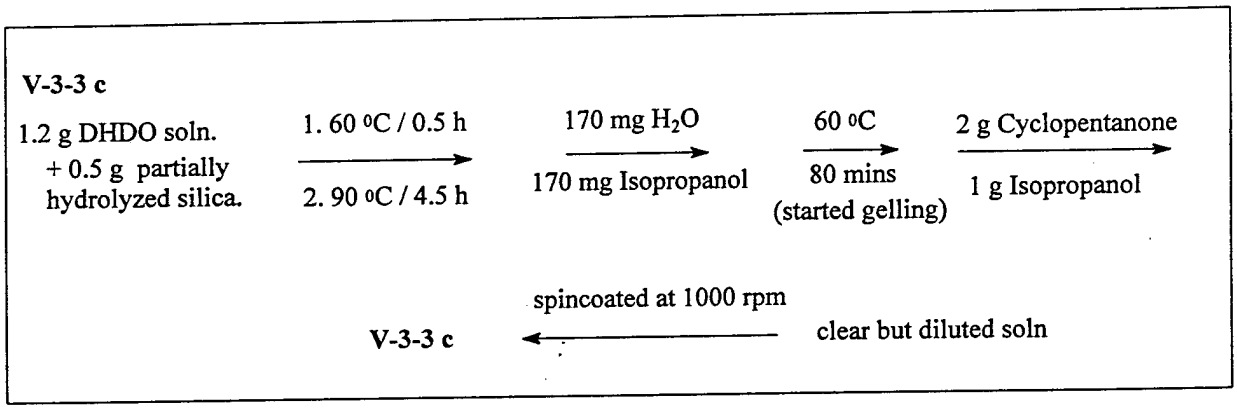

Figure III-2 Preparation of V-3-3c sol-gel composite

V-5-1: Similar to IV-99-1. Films were heated under vacuum at 100 °C for 25 mins.

All the films prepared using the above three procedures did not show any SHG signal at room temperature. The signal increased sharply with temperature, and showed very high values at 180 °C. When the sample was slowly brought back to room temperature, this value dropped to almost zero.

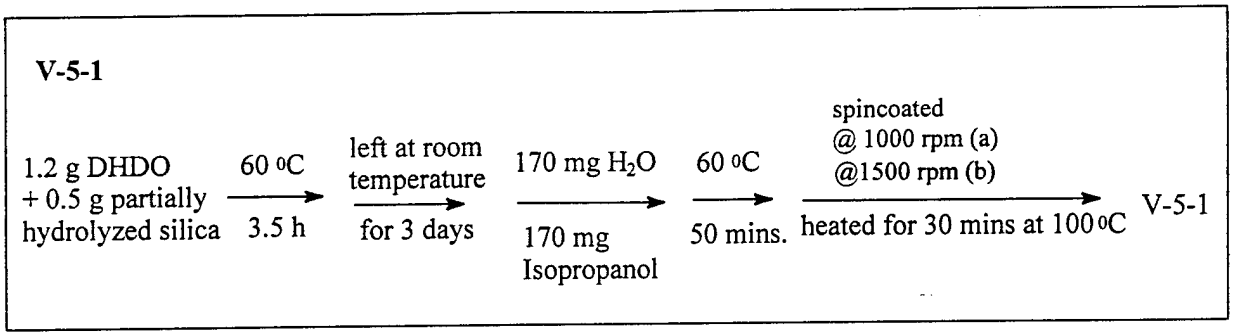

Figure III-3 Preparation of V-5-1 sol-gel composite

V-10-3b: A 39% aqueous formic acid solution containing 2 molar equivalent water for each triethoxysilane group, was added to DHDO solution in isopropanol. The solution was heated at 60 °C, cooled and mixed with partially hydrolyzed silica followed by addition of butanol and cyclopentanone. The films were spincoated and dried under vacuum at 100 °C for 2.5 h.

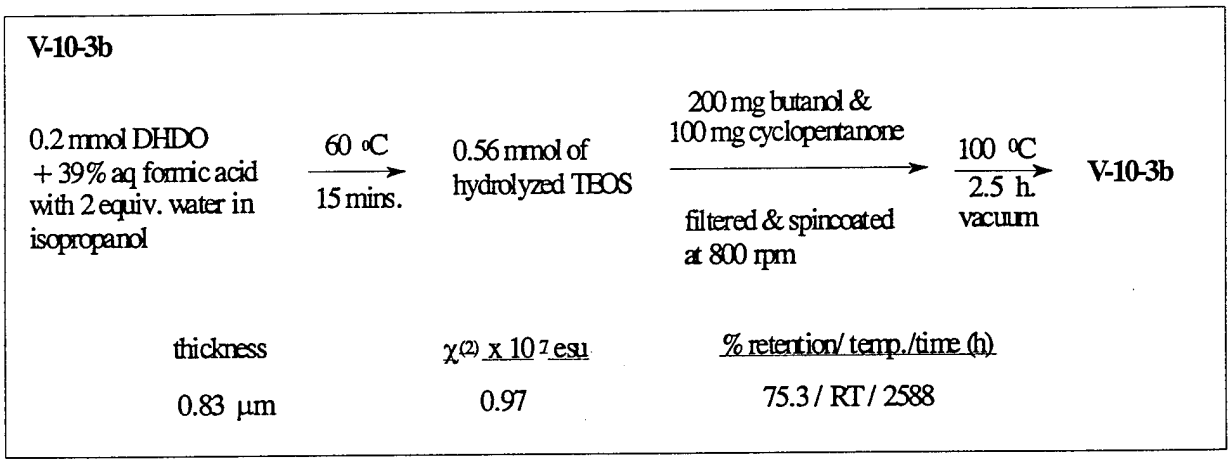

Figure III-4 Preparation V-10-3b sol-gel composite

V-11-2: A 88% aqueous formic acid solution containing 3 molar equivalents of water for each triethoxysilane group was added to a DHDO solution in isopropanol. The solution was sonicated and heated at 60 °C. The films were spincoated and dried under vacuum at 100 °C for 2.5 h.

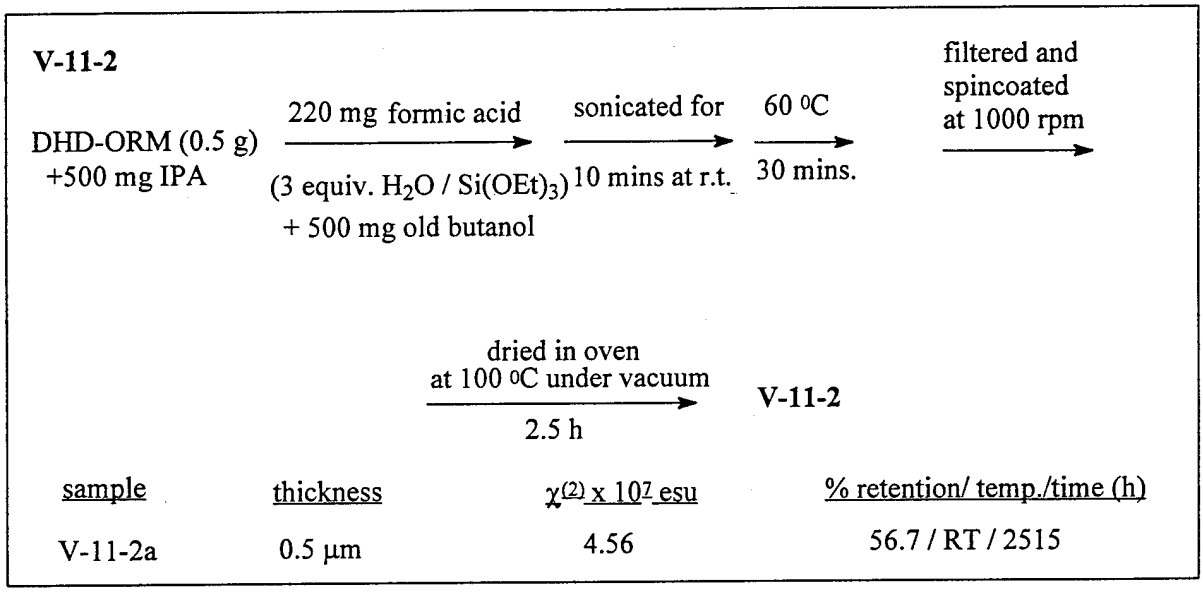

Figure III-5 Preparation of V-11-2 sol-gel composite

V-16-1: A similar procedure as above was followed. Chlorobenzene was present in the system which caused precipitation of the ormosil after hydrolysis. Cyclopentanone was added to dissolve the precipitated ormosil.

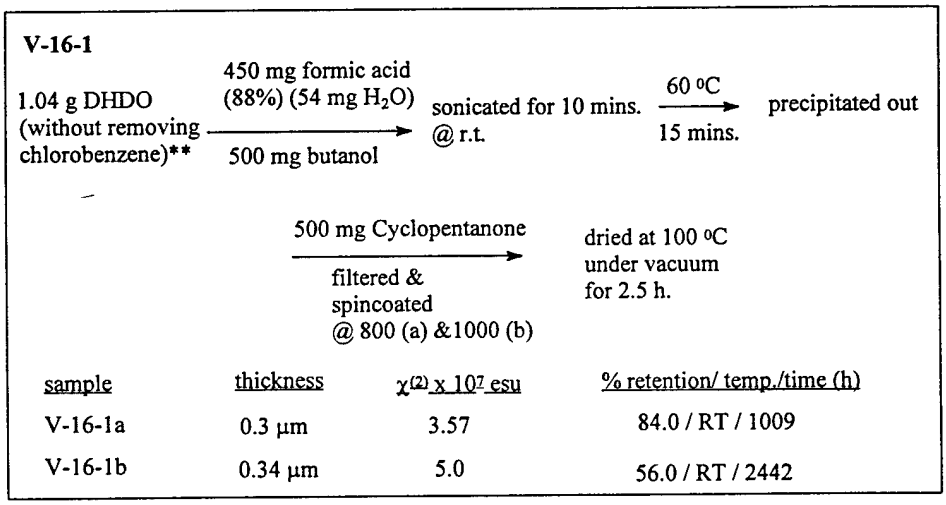

Figure III-6: Preparation of V-16-1 sol-gel composite

V-18-1: Same procedure as V-11-2.

V-18-1

DHDO soln. in isopropanol → (450 mg formic acid (88%) (54 mg H_2O); 500 mg butanol) → sonicated for 10 mins. @ room temperature → 60 °C, 5 mins → spincoated @ 900 rpm → dried under vacuum for 2.5 h @ 100 °C

sample	thickness	$\chi^{(2)}$ x 10^7 esu	% retention/ temp./time (h)
V-18-1a	0.72 μm	3.5	84.0 / RT / 2345
V-18-1b	0.71 μm	3.4	56.0 / RT / 2301
V-18-1c	0.68 μm	3.3	75.8 / RT / 2277

Figure III-7 Preparation of V-18-1 sol-gel composite

V-21-1: The procedure was the same as V-11-2. Except that butanol was added just before spincoating the film, to ease the filtration.

sample	thickness	$\chi^{(2)}$ x 10^7 esu	% retention/ temp./time (h)
V-21-1b	0.54 μm	3.9	64.1 / RT / 2325

Figure III-8 Preparation of V-21-1 sol-gel composite

V-24-1: same as V-11-2

sample	thickness	$\chi^{(2)}$ x 10^7 esu	% retention/ temp./time (h)
V-24-1b	2.6 μm	0.6	45.0 / RT / 2253
V-24-1c	1.5 μm	1.0	61.0 / RT / 1963

Figure III-9 Preparation of V-24-1 sol-gel composite

V-33-1

0.33 mmol DHD-ORM (1 mmol $Si(OEt)_3$) + 3 equiv. water (of $Si(OEt)_3$) from 88 % formic acid in butanol → sonicated for 10 mins. → 60 °C for 2 mins. → filtered through 0.2 μm & spincoated at 600 rpm → 100 °C, 2.5 h vacuum → V-33-1

sample	thickness	$\chi^{(2)}$ x 10^7 esu	% retention/ temp./time (h)
V-33-1	0.88 μm	2.8	71.4 / RT / 2063

Figure III-10 Preparation of V-33-1 sol-gel composite

V-44-2

0.33 mmol DHD-ORM soln. in butanol + 3 equiv. water (of $Si(OEt)_3$) from 88 % formic acid in 500 mg butanol → sonicated for 8 mins. → at room temp. → 0.25 equiv. (of each $Si(OEt)_3$ group) hydrolyzed silica (TMOS + 4 equiv. water + Lewis acid)

→ stirred for 1 min. → filtered through 0.2 μm & spincoated at 600 rpm → 100 °C, 1 h. under vacuum, 15 h w/o vacuum → V-80-3

sample	thickness	$\chi^{(2)}$ x 10^7 esu	% retention/ temp./time (h)
V-44-2	1.25 μm	1.2	74.2 / RT / 1632

Figure III-11 Preparation of V-44-2 sol-gel composite

V-45-1

0.33 mmol DHD-ORM soln. in butanol + 3 equiv. water from 88 % formic acid in butanol → (sonicated for 5 mins. at room temp.) → 0.25 equiv. hydrolyzed silica (TMOS + 4 equiv. water + Lewis acid catalyst)

→ (stirred for 1 min.) → filtered through 0.2 μm & spincoated at 600 rpm → (100 °C; 1 h under vacuum; 15 h at room pressure) → V-45-1

sample	thickness	$\chi^{(2)}$ x 10^7 esu	% retention/ temp./time (h)
V-45-1	1.75 μm	2.3	87.0 / RT / 2033

Figure III-12 Preparation of V-45-1 sol-gel composite

V-49-1

0.33 mmol DHD-ORM (1 mmol $Si(OEt)_3$) + 3 equiv. water (of $Si(OEt)_3$) from 0.1 M HCl in butanol → (sonicated for 20 mins. 500 mg butanol added) → filtered through 0.2 μm & spincoated at 600 rpm → (100 °C; 2.5 h vacuum) → V-49-1

sample	thickness	$\chi^{(2)}$ x 10^7 esu	% retention/ temp./time (h)
V-49-1a	2.1 μm	1.3	75.0 / RT / 675

Figure III-13 Preparation of V-49-1a sol-gel composite

V-69-1

0.33 mmol DHD-ORM (1 mmol $Si(OEt)_3$) + 3 equiv. water (of $Si(OEt)_3$) from 88 % formic acid in butanol → sonicated for 4 mins. → filtered through 0.45 µm & spincoated at 800 rpm → 80 °C, 44 h → V-69-1

sample	thickness	$\chi^{(2)}$ x 10^7 esu	% retention/ temp./time (h)
V-69-1	1.18 µm	2.9	69.0 / RT / 409
V-69-1a	1.03 µm	3.3	90.9 / RT / 233

Figure III-14 Preparation of V-69-1 sol-gel composite

V-72-1

0.33 mmol 3-(trimethoxysilyl)propyl methacrylate (V-69-2) + 1 mmol $Si(OEt)_3$ in DHD-ORM soln. in butanol + 0.015 equiv. Lewis acid in butanol → stirred for 30 mins. → 3 equiv. water in butanol was added → sonicated for 3 mins. → filtered through 0.45 µm & spincoated at 600 rpm → 80 °C, 15 h → V-72-1

sample	thickness	$\chi^{(2)}$ x 10^7 esu	% retention/ temp./time (h)
V-72-1	1.34 µm	1.9	73.7 / RT / 473

Figure III-15 Preparation of V-72-1 sol-gel composite

V-73-1

0.33 mmol DHD-ORM soln. in butanol + 3 equiv. water from 88 % formic acid in 500 mg butanol —(sonicated for 4 mins. at room temp.)→ filtered through 0.45 μm & spincoated at 800 rpm —(80 °C, 92 h. under vacuum)→ V-73-1

sample	thickness	$\chi^{(2)}$ x 10^7 esu	% retention/ temp./time (h)
V-73-1	0.97 μm	1.9	78.9 / RT / 623
V-73-1a	0.95 μm	2.8	75.0 / RT / 450
V-73-1h	1.46 μm	2.1	81.0 / RT / 474

Figure III-16: Preparation of V-73-1 sol-gel composite

V-80-3: To a solution of 0.33 mmol DHDO (containing 0.33 mmol $Si(OEt)_3$ unit) a mixture of 450 mg 88 % formic acid (containing 54 mg, i.e. 3 equiv. water) and 500 mg butanol was added and sonicated for 3 mins. at room temperature. Prehydrolyzed TEOS was added to it and stirred for a minute after which it was filtered and spincoated at 600 rpm on an ITO coated glass substrate.

V-80-3

0.33 mmol DHD-ORM soln. in butanol + 3 equiv. water from 88 % formic acid in 500 mg butanol —(sonicated for 3 mins. at room temp.)→ 0.4 equiv. (of each $Si(OEt)_3$ group) hydrolyzed silica (TEOS + 4 equiv. water + dil. HCl)

—(stirred for 1 min.)→ filtered through 0.2 μm & spincoated at 600 rpm —(80 °C, 64 h. under vacuum)→ V-80-3

sample	thickness	$\chi^{(2)}$ x 10^7 esu	% retention/ temp./time (h)
V-80-3	0.9 μm	2.3	96.0 / RT / 358
V-80-3a	0.8 μm	2.7	88.9 / RT / 358

Figure III-17 Preparation of V-80-3 sol-gel composite

V-91-3: To a solution of DHDO in butanol, 30 mg methanol was added and stirred for 15 mins. A mixture of 54 mg 0.1 M HCl and 200 mg butanol was added dropwise and stirred for 5 mins. and then sonicated for 2 mins. A mixture of 70 mg TMOS and 80 mg butanol was added to it and stirred for 5 mins. The final mixture was filtered through 0.45 μm filter and spincoated on ITO coated glass substrate at 600, 800, and 1000 rpm, followed by heating at 60 °C for 1 h.

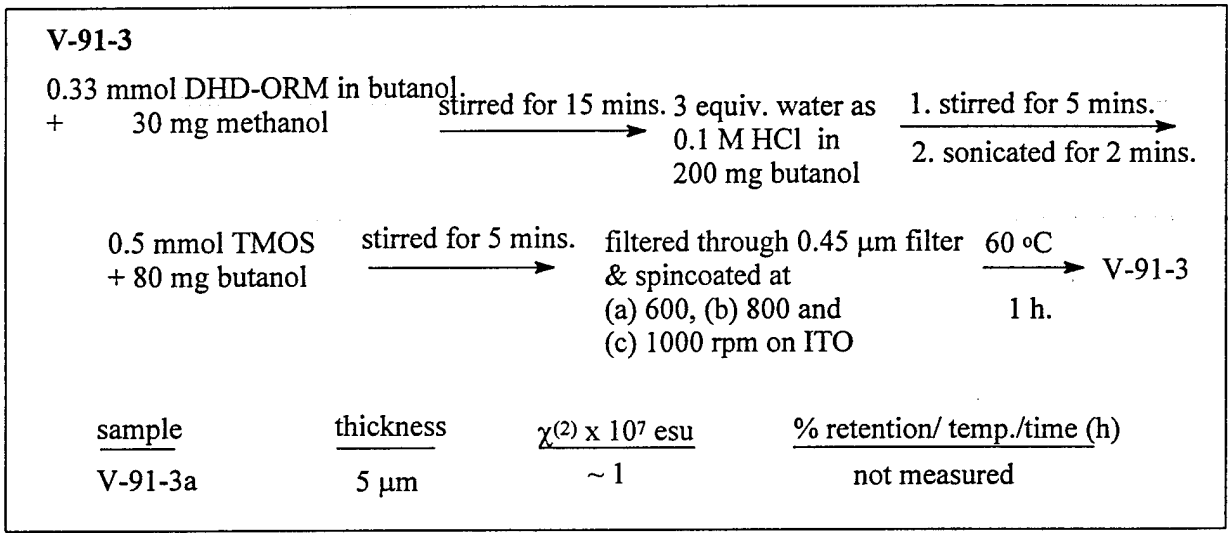

Figure III-18 Preparation of V-91-3 sol-gel composite

V-92-3: To a mixture of DHDO and butanol, 82 mg of 3-(trimethoxysilyl)propyl methacrylate (0.33 mmol of $Si(OEt)_3$) was added. Catalytic amount of Lewis acid catalyst was added and stirred for 30 mins. followed by addition of a mixture of 60 mg water in 200 mg butanol. The final mixture was stirred for 15 mins. and sonicated for 15 mins., which was then filtered and spincoated on ITO slide at 800 rpm. One film was dried at 100 °C under vacuum for 1 h and two others (a) for 7 h.

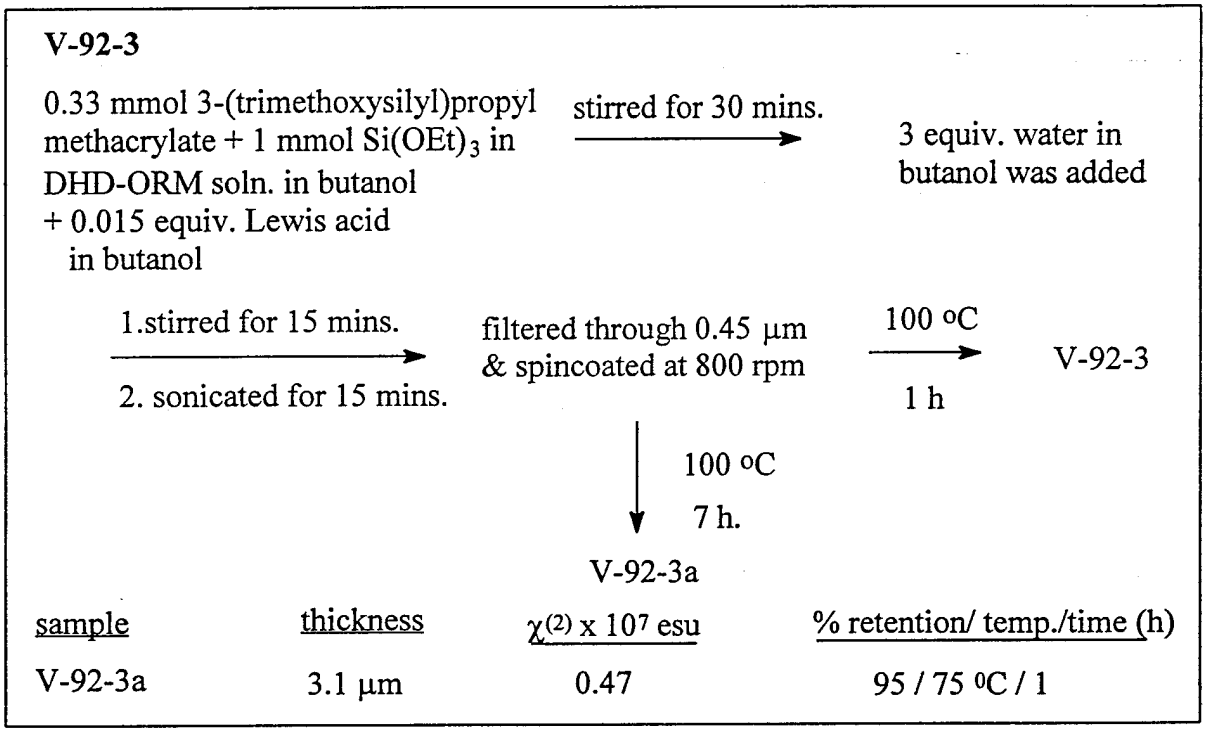

Figure III-19 Preparation of V-92-3 composites

III.3. Preparation of THS composite films

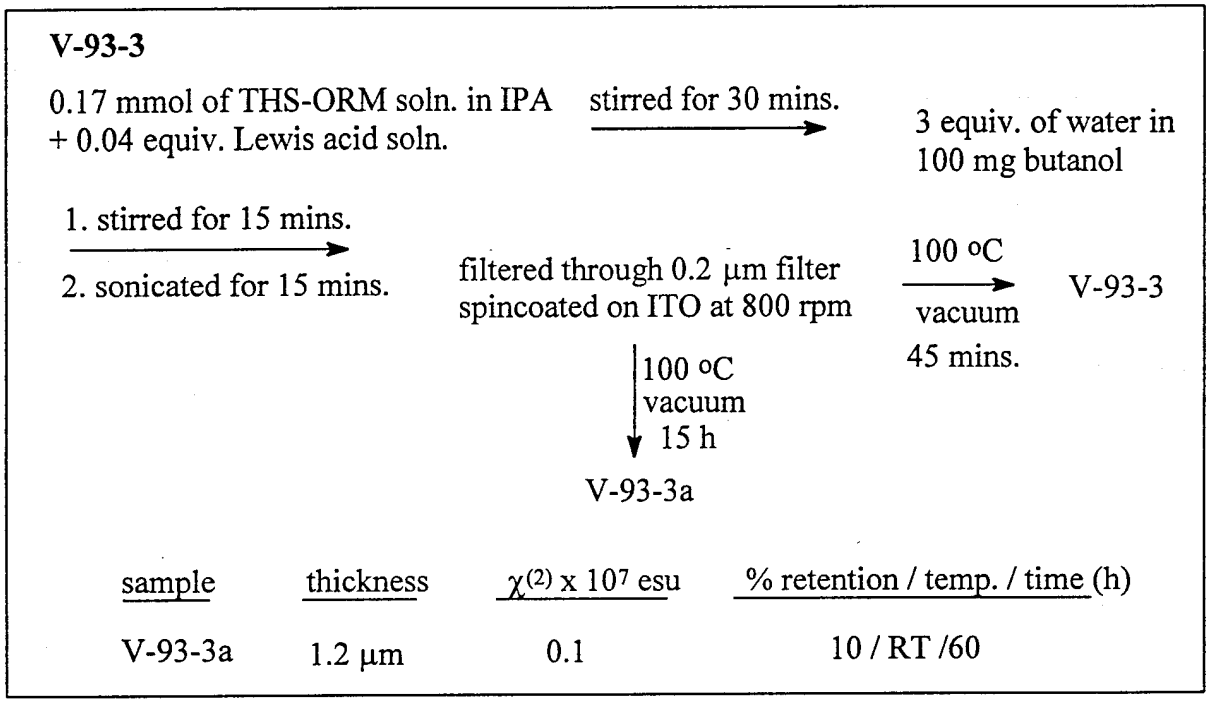

Figure III-20 Preparation of V-93-3 sol-gel composite

References:

III-1. R.J. Jeng, Y. M. Chen, A. K. Jain, S. K. Tripathy, and J. Kumar, *Optics Commun.* **89**, 212 (1992).

III-2. R.J. Jeng, Y. M. Chen, A. K. Jain, J. Kumar, and S. K. Tripathy, *Chem. Mater.*, to be published.